Temperature Dependence of the Electric Field Modulation of Electron-Transfer Rates: Charge Recombination in Photosynthetic Reaction Centers

Stefan Franzen and Steven G. Boxer*

Department of Chemistry, Stanford University, Stanford, California 94305

Received: February 19, 1993

The rates of electron-transfer reactions can be systematically varied by application of external electric fields. The electric field effect on the charge recombination rate constant of the state $P^+Q_A^-$ in photosynthetic reaction centers has been measured in polymer film samples at a number of temperatures. This extends an earlier study at 80 K in which a small field-induced slowing of the rate constant was reported [Franzen, S.; Goldstein, R. F.; Boxer, S. G. *J. Phys. Chem.* **1990**, *94*, 5135–5149]. At temperatures greater than 160 K, evidence is presented for an electric-field-induced activated recombination pathway similar to that observed in reaction centers which have nonnative quinones of low reduction potential substituted for ubiquinone. However, it is shown that this pathway alone cannot account for the electric-field-induced changes in kinetics observed at higher temperatures. The data analysis used to obtain the $\log(k_{et})$ vs ΔG_{et} curve at 80 K is extended to include changes in the steady-state population of $P^+Q_A^-$ observed at higher temperatures with a continuous wave probe beam. This field dependence is analyzed in terms of electron-transfer theory including the entropy of reaction and the temperature dependences of the reorganization energy and the local field correction. The data and analysis suggest that a temperature-dependent reorganization energy is associated with solvation of the $P^+Q_A^-$ dipole.

1. Introduction

The electric field dependence of electron-transfer (ET) rate constants can be used to obtain information on the coupling of nuclear motion to ET reactions.[1] The displacement of the nuclei which accompany an ET reaction affects the probability of reaching a nuclear configuration where the reactant and product states have the same energy and ET can occur. For some reactions, it is convenient to express the dependence of the ET rate constant k_{et} on the nuclear transition probability or nuclear factor in terms of an activation barrier.[2] When a strong or activated temperature dependence is observed, the magnitude of the barrier height or activation free energy can be obtained from the slope of a plot of $\log(k_{et})$ vs $1/T$.[3,4] Using Marcus theory, the reorganization energy λ can be calculated from the activation free energy[5] provided the free energy of reaction ΔG_{et} is known. In contrast, a mild temperature dependence is difficult to interpret unambiguously. If a reaction is relatively temperature independent, it can be argued that the reaction is activationless ($\lambda \simeq -\Delta G_{et}$),[6] in the inverted region ($\lambda > -\Delta G_{et}$)[7-9] or in the normal region if the system is coupled to largely frozen-out vibrations. The temperature dependence alone does not yield enough information to uniquely determine λ or the parameters of even a single-mode coupled to the ET process.[10] In this paper, electric fields and temperature are combined to obtain information on nuclear coupling to the $P^+Q_A^-$ recombination rate constant in bacterial reaction centers (RCs). It will be shown that electric field effect experiments can be used to determine λ even when the temperature dependence is mild.

Many studies of the temperature dependence of ET reactions have utilized RCs.[11-13] This is due in part to the fact that many of the ET reactions in RCs proceed at all temperatures studied (down to 1.5 K). The protein solvent which holds the reacting molecules in place in the RC has been structurally characterized.[14-16] The reaction scheme shown in Figure 1 applies to RCs which contain a single ubiquinone acceptor Q_A. The charge recombination (CR) reaction $P^+Q_A^- \rightarrow PQ_A$, with rate constant k_R, depends weakly on temperature, increasing by a factor of 4 as the temperature is lowered from room temperature to 77 K in glycerol/buffer solution.[12,18] The charge separation (CS) which generates the $P^+Q_A^-$ state involves at least two rapid steps after the absorption of a photon to form the state $^1PHQ_A$. The rate constant for the process $^1PHQ_A \rightarrow P^+H^-Q_A$ increases from $(3.3\ ps)^{-1}$ at room temperature to $(1.4\ ps)^{-1}$ at 77 K.[19] $P^+HQ_A^-$ is formed from $P^+H^-Q_A$ with a rate constant k_Q of $(200\ ps)^{-1}$ at room temperature which increases to about $(100\ ps)^{-1}$ at 77 K.[20,21] None of these reactions exhibit Arrhenius-type activation at any temperature. Thus, the three ET reactions observed in Q_A-containing RCs are often assumed to be activationless. However, as discussed elsewhere, this assumption does not explain the temperature dependence of these reactions in terms of ET theory.[12,22] For example, both the primary charge separation and the $P^+Q_A^-$ recombination rates increase as the temperature is lowered more rapidly than predicted by ET theory.

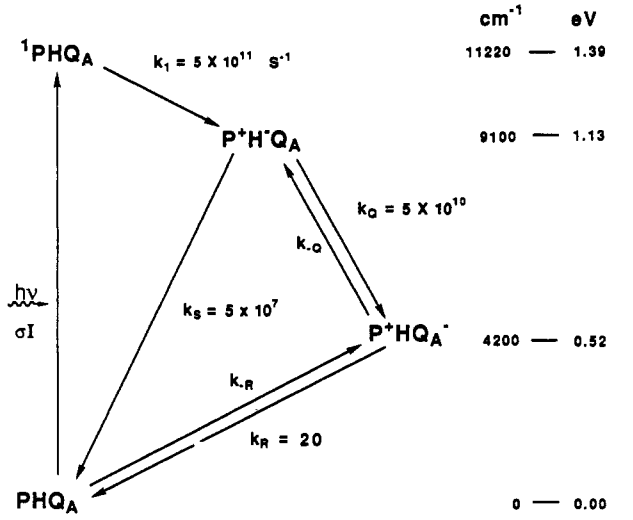

Figure 1. Reaction scheme for quinone-containing RCs. The energies of the states are shown on the right in cm^{-1} and eV. The energy used for the P^+H^- state is based on the experiments of ref 17 although a value of 1.07 eV may be appropriate for the activated back reaction via k_{-Q}.[25] The absorption of a photon to form ^1P is indicated by an effective rate constant σI (σ is the absorption cross section and I is the probe intensity).

At higher temperatures, an activated reaction involving an equilibrium between the states $P^+Q_A^-$ and P^+H^- has been observed in RCs from *Rps. viridis*[23] or in *Rb. sphaeroides* when nonnative

0022-3654/93/2097-6304$04.00/0 © 1993 American Chemical Society

anthraquinone (AQ) is substituted for the native ubiquinone.[24] The free energy of the $P^+Q_A^-$ recombination with nonnative AQ is altered such that the energy gap from $P^+Q_A^-$ to P^+H^- is about 0.2 eV smaller than for native ubiquinone.[25,26] In an applied electric field, if the energy of the $P^+Q_A^-$ state is shifted close enough to the P^+H^- state, the activated pathway can compete with the direct CR pathway. Evidence for such a process has been presented in the electric field effect experiments of Gopher et al.[26] where the effect of the applied field on native ubiquinone yielded a relatively small field dependence, but the electric field effect on AQ-substituted RCs showed a large field dependence, indicating that CR is in part activated for this quinone. The probable origin of the electric-field-induced recombination involves equilibrium of $P^+Q_A^-$ with P^+H^- which has a decay rate constant $k_S \simeq 5 \times 10^7\ s^{-1}$ at room temperature.[25] k_S slows by approximately a factor of 4 between 290 and 77 K.[27,28] The electric field dependence of k_S is not known and may also play a role in the observed activated process. Since the rate constant k_Q is a factor of 70 times larger than k_S (and larger still at lower temperatures), the quantum yield for the formation of the state $P^+Q_A^-$ is expected to be close to one in agreement with experiment.[29]

Electric field effect experiments on the $P^+Q_A^-$ CR reaction have been reported at room temperature in oriented samples[26,32,33] and at 80 K in isotropic samples.[1] The experiments in this paper extend the range of the electric field effect experiments in isotropic thin polymer film samples from 80 to 290 K. The results presented below will be compared directly to the electric field effect measurements of Gopher et al.,[26] Feher et al.,[32] and Popovic et al.,[33] as well as the quinone substitution data of Gunner et al.[8,34]

2. Experimental Section

Reaction centers from *Rb. sphaeroides* R-26 were obtained by standard methods.[35] In cases where Q_B was detected based on the observed kinetics, the Q_B depletion procedure of Okamura was used to prepare the RCs with a single ubiquinone in the Q_A site.[36] Thin poly(vinyl alcohol) (PVA) film sample preparation and the apparatus are described in ref 1. Samples had thicknesses ranging from 4.0 ± 0.15 to 7.0 ± 0.25 μm as measured with a Sloan Dektak IIa thickness measuring system (precision ±0.1 μm) and had optical densities ranging from 0.02 to 0.1 at 870 nm. The thinnest samples were the most homogeneous and often had no detectable surface features within the accuracy of the Dektak. The capacitance of the films is sensitive to the moisture content of the polymer films. When the samples are first inserted into the closed cycle helium refrigerator used for the experiments,[1] the capacitance is observed to be about 5% higher than the value obtained after the refrigerator has been evacuated to less than 10^{-3} Torr for ca. 1 h.

The appearance of $P^+Q_A^-$ and the recovery of the ground state were monitored by observing the bleach and recovery, respectively, of the 864-nm band associated with P. The absorption band shifts to the red and narrows considerably at low temperature such that its maximum is 885 nm at 80 K. Broad band light from a tungsten halogen lamp filtered to produce a beam centered at 870 ± 40 nm was used as a probe beam. The spectral bandwidth of the near-infrared filters used for the broad-band probe was increased at higher temperatures in order to eliminate offsets due to electrochromism. Because the bandwidth of the filters which were used was broader than the absorption bandwidth, wavelengths were sampled beyond the absorption where no signal is present. As a result, the signal-to-noise ratio was poorer than that obtained earlier at 80 K where the filter was well-matched to the absorption. The probe beam was reflected off the aluminum electrode at 16.4° incidence, and the transient signal was measured with a silicon photodiode. For some experiments, a $^1/_4$-m monochromator was used to obtain a relatively narrow bandwidth probe source (5-nm bandwidth). The flash excitation source was the doubled output from a Nd:YAG laser (pulse width ~ 9 ns) whose intensity was adjusted to excite about 70% of the RCs. The high voltage (between 400 and 800 V) was gated on immediately following the excitation flash with a rise time of < 50 μs. Under these conditions, the steps forming $P^+Q_A^-$ take place in the absence of the field, and the field is on during the entire $P^+Q_A^-$ decay.

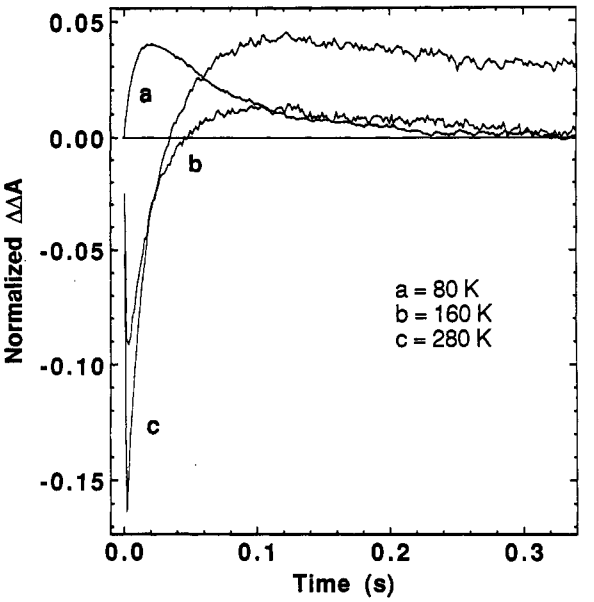

Figure 2. Temperature dependence of $P^+Q_A^-$ recombination in an applied electric field (F = 0.9 MV/cm; probe beam broad band, $I = 30\ \mu W/cm^2$; see eq 1 for definition of $\Delta\Delta A$).

In order to test for charge injection into the sample at various temperatures, the current on the high-voltage line was monitored. A current pulse required to charge the sample lasts approximately 100 μs, and the charge required increases with temperature proportional to the sample capacitance. There was no evidence of current flow at any time during the application of the voltage except during charging and discharging of the sample. The same total current flowed when the sample was flashed with the laser and when it was kept in the dark.

3. Results

3.1. Temperature Dependence of the Electric Field Effect. The temperature dependence of the electric field effect on the $P^+Q_A^-$ decay kinetics following flash excitation is shown in Figure 2 at three selected temperatures. Limited data were collected at several intermediate temperatures; for a given field, the results were intermediate between those at the temperatures shown. The signals shown in Figures 2–5 are the normalized difference, $\Delta\Delta A(\mathbf{F},t)$, the absorbance change at time t in the presence and absence of an applied electric field, $\Delta A(\mathbf{F},t)$ and $\Delta A(\mathbf{F}=0,t)$, respectively:

$$\Delta\Delta A(\mathbf{F},t) = \frac{\Delta A(\mathbf{F},t) - \Delta A(0,t)}{\Delta A(0,0)} \qquad (1)$$

The magnitude of the electric field effect shown in Figure 2 increases as the temperature increases, both in the negative component at times less than 100 ms (faster rates) and in the positive component (slower rates). Note that $\Delta\Delta A$ does not return to the original baseline at 290 K. This is due to a field-dependent shift in the steady-state concentration of $P^+Q_A^-$ produced by the probe beam only. This novel phenomenon and several related effects are discussed in detail in the Appendices.

The response of the sample to the application of the field with or without flash excitation at 290 K is shown in Figure 3. When the bias of the applied voltage is reversed, there is an abrupt change in both signals. Both difference decays show nearly the same $\Delta\Delta A$ after 400 ms. A broad-band probe beam was used

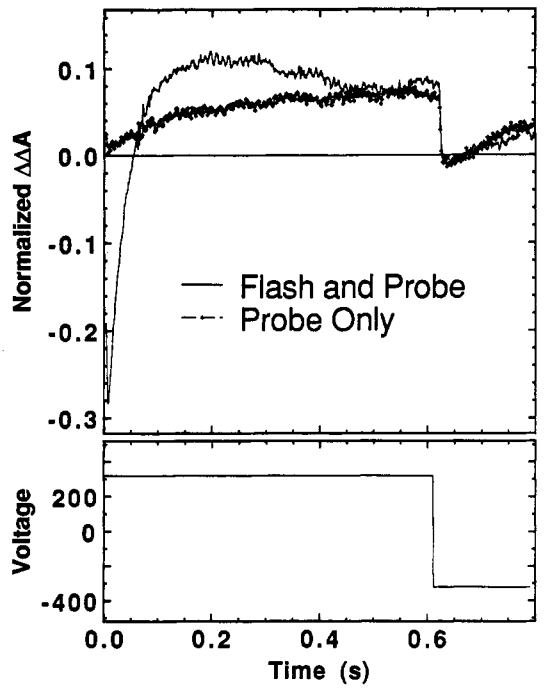

Figure 3. Comparison of electric field effect on the $P^+Q_A^-$ concentration with and without laser flash excitation at 290 K (F = 0.92 MV/cm; probe beam I = 150 μW/cm^2). The electric field effect with a probe alone is shown as $\Delta A(F,t)/\Delta A(0,0)$ for comparison with the flash data which are a normalized $\Delta\Delta A$ given by eq 1.

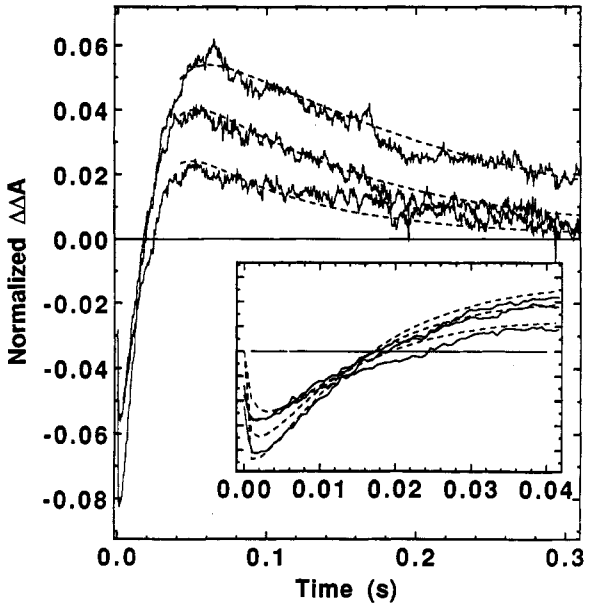

Figure 4. $\Delta\Delta A$ as a function of time and applied electric field for $P^+Q_A^-$ recombination at 160 K (probe beam I = 150 μW/cm^2; F = 0.83, 0.95, and 1.05 MV/cm with the effect increasing as the field increases). The dashed line is the fit to the data using eq 3. The early time data are shown in the inset with the indicated expanded time base and the same ordinate scale as the full time base plot.

to exclude the possibility that the change in the baseline is due to the electrochromism of P[37,38] (see Appendix A).

Temperatures 160 and 290 K were selected for more detailed electric field dependence measurements. Along with the original 80 K, data at these three temperatures illustrate the major differences observed with temperature. The data obtained at 160 and 290 K when a sample has been excited with a laser flash and an electric field has been applied after the flash are shown in Figures 4 and 5 (six field values were examined; only three are shown for clarity of presentation). The magnitude of the effect of the electric field on the kinetics increases in a nonlinear fashion as the field is increased. The effect of an applied electric field

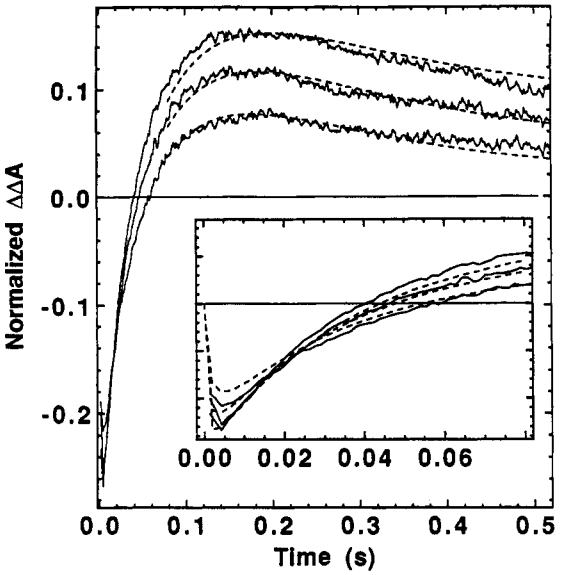

Figure 5. $\Delta\Delta A$ as a function of time and applied electric field for $P^+Q_A^-$ recombination at 290 K (probe beam I = 150 μW/cm^2; F = 0.75, 0.89, and 1.03 MV/cm with the effect increasing as the field increases). The dashed line is the fit to the data using eq 3. The early time data are shown in the inset with the indicated expanded time base and the same ordinate scale as the full time base plot.

is larger at 290 K than at 160 K at all values of the applied electric field.

3.2. Temperature Dependence of the Dielectric Constant. The dielectric constant ϵ of the sample is required in order to calculate the local field correction.[39] The temperature dependence of ϵ of the PVA film can be estimated from a measurement of the temperature dependence of the capacitance ($\epsilon \propto A/[dC]$ where A is the electrode area, d is the distance between the electrodes, and C is the sample capacitance). Assuming the dielectric constant at 80 K is 4 as was found by Lösche et al.[38] ($\epsilon_{PVA} \simeq 4$ at 77 K), the dielectric constant increases to 8 at 290 K in our samples compared to $\epsilon_{PVA} \simeq 10$ at 295 K in ref 38. This difference may reflect the additional drying of the PVA films due to the applied vacuum necessary to reach high electric fields in our experimental apparatus.

3.3. Temperature Dependence of the Zero-Field Rate Constant. At 80 K, $P^+Q_A^-$ CR is made up of at least two single-exponential processes which occur in parallel.[40] For convenience, these will be referred to as population 1 (the faster population) and population 2 (the slower population). The average rate of the recombination reaction slows down by a factor of 2 as the temperature is increased from 80 to 290 K. The slow process (population 2) contributes most to the temperature dependence, and the ratio of the two populations changes from 60:40 (fast:slow) at 80 K to 40:60 (fast:slow) at 290 K.

4. Methods of Analysis

4.1. Dependence of the Rate Constant on Electric Field. The first step in the data analysis consists of fitting the kinetic data obtained in an electric field to a general model function: a cumulant expansion. Using this description, the electric-field-dependent ET rate constant is

$$k_{et}(\mathbf{F}) = \exp\{\sum_{n=0}^{\infty} P_n(\Delta U)^n\} \qquad (2)$$

where $\Delta U = -\Delta\mu_{et}\cdot\mathbf{F}$, $\Delta\mu_{et}$ is the difference electric dipole moment between the reactant and product states, and $\mathbf{F}$ is the internal applied electric field. Once obtained from a fit to the data, the parameters P_n are used to generate a rate vs interaction energy [$\log(k_{et})$ vs ΔU] curve. The zeroth cumulant corresponds to the zero-field rate, $k(0) = \exp(P_0)$.

The electric-field-induced change in the absence of laser flash excitation shown in Figure 3 can be attributed to a change in the $P^+Q_A^-$ steady-state concentration (see Appendix A). The data analysis used to obtain the parameters P_n must include the change in steady-state concentration using eq B.6 (Appendix B). Because there are two populations of RCs observed at zero electric field at all temperatures, a steady-state term is added to each population, and the result is averaged over all orientations of $\Delta\mu_{et}$

$$\Delta\Delta A(\mathbf{F},t) = \sum_{i=1}^{2}\left[\int_{-1}^{1} d(\cos\theta)\,\exp\{-k_{Ri}(\mathbf{F})t\} - \exp\{-k_{Ri}(0)t\} + \frac{1}{S}\int_{-1}^{1} d(\cos\theta)[1-\exp\{-k_{Ri}(\mathbf{F})t\}]I\times\left\{\frac{\sigma(\mathbf{F})\Phi(\mathbf{F})}{k_{Ri}(\mathbf{F})+\sigma(\mathbf{F})\Phi(\mathbf{F})I} - \frac{\sigma(0)}{k_{Ri}(0)+\sigma(0)I}\right\}\right] \quad (3)$$

where $k_{R1}(\mathbf{F}) = \exp\{\sum_n P_n(\Delta U)^n\}$ and $k_{R2}(\mathbf{F}) = \exp\{\sum_n Q_n(\Delta U)^n\}$ represent the electric-field-dependent rate constants of populations 1 and 2, respectively, θ is the angle between $\Delta\mu_{et}$ and $\mathbf{F}$, I is the probe beam intensity, $\sigma(\mathbf{F})$ and $\Phi(\mathbf{F})$ are the field-dependent absorption cross section and $P^+Q_A^-$ quantum yield, respectively (see Appendix B), and S is the saturation factor, $\Delta A(0,0)/A(0,0)$, where $A(0,0)$ is the absorbance of the sample at the probe wavelength. The parameters used are called P_n for population 1 and Q_n for population 2 as in ref 1. The observed signal is affected by the experimental angle χ between the electric vector probe beam and the applied field $\mathbf{F}$ as described in ref 1.

The second step in the data analysis is the comparison of the rate vs interaction energy curve with theory. We shall assume that the entropy of the reaction does not depend on electric field (see section 4.3), in which case the $\log(k_{et})$ vs ΔU curve is also a $\log(k_{et})$ vs ΔG_{et} curve. In principle, for a two-state system, the cumulants P_n (and Q_n) obtained from the fit of the data can be related to the moments of an expansion of the quantum-mechanical expression for the rate constant.[45] If the reaction is not a two-state system, the interpretation of these curves is more complicated due to the involvement of other states in the reaction scheme and temperature-dependent dynamics of the system (see Appendix B). In the following, the electric-field-induced change in the quantum mechanical rate constant of $P^+Q_A^-$ CR will be treated separately from the change in rate due to the thermally activated pathway via P^+H^-. In the limit of small applied field, the contribution from the activated pathway via P^+H^- to the rate will be small (based on the energetics and kinetics known from comparable quinone substitutions discussed below). Thus, in the small electric field limit, we can base the analysis only on the first parameter: the slope of the rate vs free-energy curve, P_1 or Q_1 for population 1 or 2, respectively. This is also the most overdetermined parameter obtained from the fit to the kinetic data in Figures 4 and 5 at 160 and 290 K, respectively.

4.2. Relationship to Marcus Theory. Using the result which has been derived from first-order time-dependent perturbation theory and assuming the Born–Oppenheimer and Condon approximations, the rate constant can be written as[46]

$$k_{et} = \frac{2\pi}{\hbar}|V^2|\mathrm{FC} \quad (4)$$

where $\hbar$ is Planck's constant, V is the electronic coupling, and FC is the Franck–Condon weighted density of states. In most applications of this expression to the temperature dependence of ET rates, it has been assumed that the temperature dependence is contained only in the term FC. The electronic coupling may be a function of temperature if the distance changes due to thermal contraction. This has been suggested in ref 12 but has not yet been demonstrated for the RC. If a single set of parameters (e.g., those found at low temperature in ref 1) cannot fit the direct ET data at higher temperatures, the temperature dependence of the free energy and/or reorganization energy may be involved.

The information content of the data can be expressed in terms of the number of parameters uniquely determined by either an electric field effect experiment or a temperature-dependence experiment. The number of parameters in an ET theory which can be determined from an experiment is equal the minimum number of moments in an expansion of the rate constant (in powers of either energy or temperature) which are required to adequately fit the data. In general, one can expand the FC factor as a cumulant expansion in either energy or temperature:

$$\mathrm{FC}(\Delta G) = \exp\{\chi_{G0} + \chi_{G1}(\Delta G - \Delta G_{et}) + {}^1/_2\chi_{G2}(\Delta G - \Delta G_{et})^2 + ...\} \quad (5a)$$

$$\mathrm{FC}(T) = \exp\{\chi_{T0} + \chi_{T1}(T - T_0) + {}^1/_2\chi_{T2}(T - T_0)^2 + ...\} \quad (5b)$$

where χ_{Gn} and χ_{Tn} are the nth cumulant of free energy or temperature, respectively. These cumulant expressions differ from the formal definition by a factor $-i^n$ for the nth cumulant.[45] For temperature-dependent data, the cumulants are obtained by fitting the data plotted as $\log(k_{et})$ vs T to a polynomial. For electric field effect data, the procedure for obtaining the cumulants from the data is discussed in ref 1, along with the assumptions used in considering the energy change in the applied field ΔU as a contribution to the free energy.

The FC factor from dielectric continuum theory can be used to develop an application of eqs 5a and 5b which uses only the information contained in the slope of the rate vs ΔG_{et} curve:[2]

$$\mathrm{FC} = \frac{1}{[4\pi\lambda kT]^{1/2}}\exp\left\{-\frac{\Delta G^*}{kT}\right\} \quad \text{with} \quad \Delta G^* = \frac{(\lambda + \Delta G_{et})^2}{4\lambda} \quad (6)$$

where λ is the sum of energetic contributions of all of the modes which are coupled to the ET reaction. The barrier height is given by the activation free energy ΔG^*.

The FC factor in Marcus theory is Gaussian in the free energy ΔG_{et}, and therefore, there are at most two cumulants in the energy. The first cumulant in free energy χ_{G1} is

$$\frac{\partial\log(\mathrm{FC})}{\partial\Delta G_{et}} = -\frac{1}{2kT}\left[1 + \frac{\Delta G_{et}}{\lambda}\right] \quad (7)$$

which contains the electrochemical transfer coefficient $\alpha = -{}^1/_2(1 + \Delta G_{et}/\lambda)$ as described in the appendix to ref 1. The first cumulant in temperature χ_{T1} is

$$\frac{\partial\log(\mathrm{FC})}{\partial T} = \frac{1}{T_0}\left[\frac{(\lambda + \Delta G_{et})^2}{4\lambda kT_0} - \frac{1}{2}\right] \quad (8)$$

For $\Delta G^* \neq 0$, eq 8 gives the linear part of the Arrhenius dependence of $\log(k_{et})$ on temperature. For activationless processes, $\Delta G^* = 0$, and $\log(k_{et})$ vs T has a slope of $-1/2T_0$. In either of these cases, a single cumulant in temperature χ_{T1} can be obtained. Provided ΔG_{et} is known, the reorganization energy λ can be obtained when either eq 7 is fit to rate data as a function of the free energy or eq 8 is fit to rate data as a function of temperature. A temperature dependence which is nonlinear (e.g., the much studied cytochrome oxidation reaction in bacterial RCs[7,11]) requires more than one cumulant (eq 5). Regardless of the electron-transfer theory used to calculate the temperature dependence, these is a limiting negative value to the slope given by eq 8 (if entropy is not included). This has posed problems in past attempts to fit the temperature dependence of the $P^+Q_A^-$ CR reaction in many species of photosynthetic bacteria. The increase in rate as the temperature is lowered exhibited by this CR reaction is too large to be fit quantitatively even by multiphoton

ET theory.[17] The following sections consider additional factors which may affect the temperature dependence of ET rate constants which are often neglected.

4.3. Contribution of Entropy. The fact that the temperature dependence of $P^+Q_A^-$ CR is not well represented by eq 8 may be due to the neglect of entropy. The results of delayed fluorescence measurements near room temperature[47] give a negative entropy (ΔS_{et}) change for the $P^+Q_A^- \rightarrow PQ_A$ charge-transfer reaction which is large enough to increase the magnitude of the free energy by ca. 0.08 eV between 290 and 80 K (assuming ΔS_{et} is independent of temperature).

If the entropy is included,

$$\frac{\partial \log(FC)}{\partial T} = \frac{1}{T}\left\{\left[\frac{2T\Delta S_{et}}{\lambda + \Delta G_{et}} + 1\right]\frac{\Delta G^*}{kT} - \frac{1}{2}\right\} \quad (9)$$

The first term in eq 9 contains the activation enthalpy.

$$\Delta H^* = \Delta G^*\left[1 + \frac{2T\Delta S_{et}}{\lambda + \Delta G_{et}}\right] \quad (10)$$

If $\Delta S_{et} < -(\lambda + \Delta H_{et})/T$, the activation enthalpy will be negative. Similar relationships have been considered by Sutin and Marcus for self-exchange and cross-exchange reactions of $Fe(bpy)_3^{3+}$ and $Ru(bpy)_3^{3+}$.[48]

4.4. Contribution of a Temperature-Dependent Reorganization Energy. In order to account for the observed temperature dependence of the ET rates, it may also be necessary to consider the temperature dependence of the dielectric constant as a contribution to a temperature-dependent reorganization energy. The contribution of high-frequency modes (λ_{inner}) to λ is not highly temperature dependent unless the frequencies of the modes are temperature dependent. In Marcus theory, the solvent coordinate is a polarization coordinate which is temperature dependent.[2] The magnitude of the static dielectric constant is determined by the reorientation of solvent dipoles and is therefore temperature dependent, while the high-frequency (or optical) dielectric constant is almost independent of temperature.[49] The temperature dependence of the reorganization energy is therefore due to the temperature dependence of the static dielectric constant.

For a temperature-dependent reorganization energy (as well as free energy), the first cumulant has the form

$$\frac{\partial \log(FC)}{\partial T} = \frac{1}{T}\left[\frac{\Delta H^*}{kT} - \frac{1}{2}\right] - \frac{\partial\lambda/\partial T}{\lambda}\left\{\frac{\Delta G^*(\lambda - \Delta G_{et})}{kT(\lambda + \Delta G_{et})} + \frac{1}{2}\right\} \quad (11)$$

where $\partial\lambda/\partial T$ must be determined either from experiment or from a model for the temperature dependence of the static dielectric constant empirically, and ΔH^* is defined in eq 10.

4.5. Role of Temperature Dependence of the Local Field Correction. The temperature dependence of the dielectric constant can also affect the electric field experienced by the molecules in the sample. Polarization effects can be accounted for by calculating the local field at the chromophore which is participating in the ET process. Since RCs of *Rb. sphaeroides* are approximately spherical in shape, one can use the spherical cavity approximation to obtain the local field correction inside the protein $f = 3\epsilon_{PVA}/(2\epsilon_{PVA} + \epsilon_{RC})$. The chromophores P and Q_A inside the RC are not well described by a spherical cavity. An ellipsoidal cavity approximation may be a better description; however, it is not obvious how to define the ellipsoid inside the RC, so we will use the spherical cavity approximation to obtain an upper bound value, which suffices for the purpose of comparing relative values

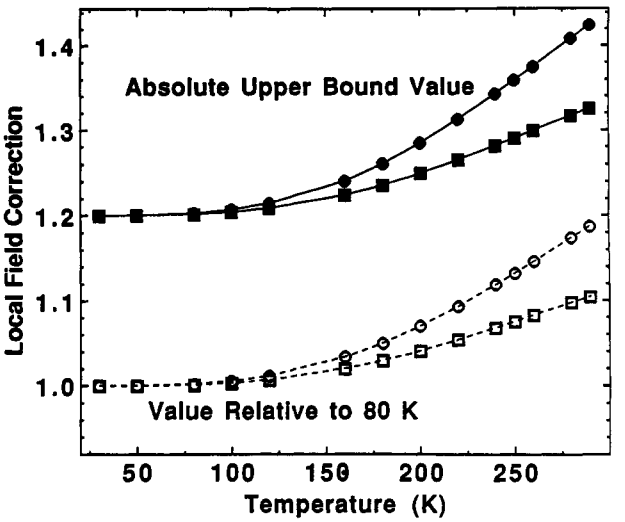

Figure 6. Relative and absolute values of the local field correction as a function of temperature. Two limiting cases, ϵ_{PVA} only varying with temperature (squares) and $\epsilon_{RC} \simeq \epsilon_{PVA}$ at all temperatures (circles), are plotted both in terms of the absolute value of the local field correction based on the upper bound value of $f = 1.2$ at 80 K (solid squares and solid circles) and relative to the 80 K value (hollow squares and hollow circles).

of f. If the dielectric constant of the chromophores is ϵ', the total local field correction is[51]

$$f = \left[\frac{3\epsilon_{PVA}}{2\epsilon_{PVA} + \epsilon_{RC}}\right]\left[\frac{3\epsilon_{RC}}{2\epsilon_{RC} + \epsilon'}\right] \quad (12)$$

The optical dielectric constant of typical aromatic molecules is about 2. The dielectric constant of PVA has been measured to be about 4 at 80 K and 8 at 290 K (see section 3.2). We are not concerned with the absolute magnitude of the local field correction but rather with the relative change with temperature. In ref 1, it was noted that the k_{et} vs ΔG_{et} curves are fit by ET theory with reasonable mode frequencies as long as $f < 1.2$ at 80 K. For purposes of comparison as a function of temperature, the upper bound of $f = 1.2$ at 80 K can be used (e.g., at 80 K, $\epsilon_{RC} = \epsilon_{PVA} = 4$ and $\epsilon' = 2$).

In order to estimate the temperature dependence, two types of behavior are considered: (i) the dielectric constant of the RC protein is assumed to be 4 at all temperatures, or (ii) the RC protein ϵ is allowed to vary in proportion to the PVA dielectric constant. If the dielectric constant of the interior of the RC is fixed at a value of 4 (case i), the local field correction inside the bulk of the RC will increase as the PVA dielectric constant increases with temperature. If both the PVA and RC dielectric constants are equal at all temperatures (a special case of ii), the local field inside the RC will not change, but the local field at the reacting species (P and Q_A) will change due to the protein dielectric. If the RC dielectric constant increases more than the PVA dielectric constant, the relative change is smaller than the special case of ii where both are always equal. The relative change in local field correction for each case is shown in Figure 6. The relative local field correction compared to 80 K is at most a factor of 1.2 larger at 290 K and a factor of 1.06 larger at 160 K.[52]

5. Results of Analysis

5.1. Determination of Rate vs ΔG_{et} Curves for $P^+Q_A^-$ Recombination. The electric-field-dependent data were fit to eq 3 using the technique described in ref 1. The experimental rate vs ΔG_{et} curves at 160 and 290 K are shown in Figure 7 calculated based on the fit to the data using six cumulants. Attempts to fit the large changes in rate in Figures 4 and 5 using only four cumulants for each rate constant were not satisfactory. An increase above 6 cumulants did not substantially improve the fit to the data (a maximum of 10 cumulants were used for comparison). The values

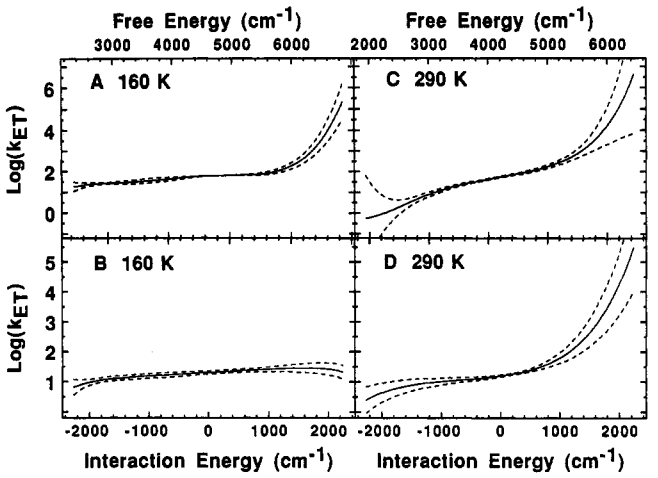

Figure 7. Experimental rate vs free-energy curves for $P^+Q_A^-$ recombination at 160 and 290 K. The errors are shown using dotted lines. (**A**) 160 K for population 1, (**B**) 160 K for population 2, (**C**) 290 K for population 1, (**D**) 290 K for population 2. See Tables I and II for the parameter values at 160 and 290 K, respectively.

TABLE I: Terms in the Cumulant Expansion and Error Analysis of Electric-Field-Modulated Kinetics at 160 K

	fast population 1			slow population 2		
n	P_n[a]	σ_P[b]	$(P_n)\Delta U^n$[c]	Q_n[a]	σ_Q[b]	$(Q^n)\Delta U^n$[c]
0	1.78	0.01	1.78	1.30	0.05	1.161
1	1.1	0.55	0.30	0.9	0.7	0.25
2	-9.4	8.3	0.74	-0.4	1.5	0.03
3	16.0	23.0	0.35	1.3	30.0	0.03
4	440.0	280.0	2.67	16.0	70.0	0.10
5	800.0	60.0	1.37	18.0	340.0	0.03
6	-900.0	2800.0	0.43	-630.0	780.0	0.30

[a] The parameters P_n and Q_n are in units of eV^{-n} for the nth cumulant appropriate for a base 10 exponential fitting function. [b] The root-mean-square deviation is σ. The calculation of the errors is described in ref 1. [c] These terms show the maximum contribution of each term in the series at the highest field which corresponds to an interaction energy of $\Delta U_{max} \simeq 0.28$ eV. The relative contribution of each term decreases with the nth power of $\Delta U/\Delta U_{max}$ for all $\Delta U < \Delta U_{max}$.

TABLE II: Terms in the Cumulant Expansion and Error Analysis of Electric-Field-Modulated Kinetics at 290 K

	fast population 1			slow population 2		
n	P_n[a]	σ_P[b]	$(P_N)\Delta U^n$[c]	Q_n[a]	σ_Q[b]	$(Q^n)\ \Delta U^n$[c]
0	1.73	0.04	1.73	1.19	0.04	1.19
1	4.1	0.2	1.14	2.10	0.60	0.58
2	0.5	5.0	0.03	11.0	4.00	0.85
3	85.0	27.0	1.86	59.0	31.0	1.28
4	30.0	100.0	0.18	140.0	79.0	0.86
5	250.0	400.0	0.43	400.0	170.0	0.68
6	2600.0	4200.0	1.23	50.0	460.0	0.02

[a] The parameters P_n and Q_n are in units of eV^{-n} for the nth cumulant appropriate for a base 10 exponential fitting function. [b] The root-mean-square deviation is σ. The calculation of the errors is described in ref 1. [c] These terms show the maximum contribution of each term in the series at the highest field which corresponds to an interaction energy of $\Delta U_{max} \simeq 0.28$ eV. The relative contribution of each term decreases with to the nth power of $\Delta U/\Delta U_{max}$ for all $\Delta U < \Delta U_{max}$.

of the cumulants and errors obtained from the best fit are given in Tables I and II. The errors given in Tables I and II are shown as the dashed lines in Figure 7. Although the errors of the higher cumulants appear large, the bounding error curves shown in Figure 7 show that these curves are well determined over most of the range of applied electric fields. The results at 160 and 290 K represent the average of five data sets obtained from four different samples. Both the observed acceleration in CR rate and the deceleration in rate which were observed in the data (Figures 4 and 5) are quantitated in *the experimental* rate vs free-energy

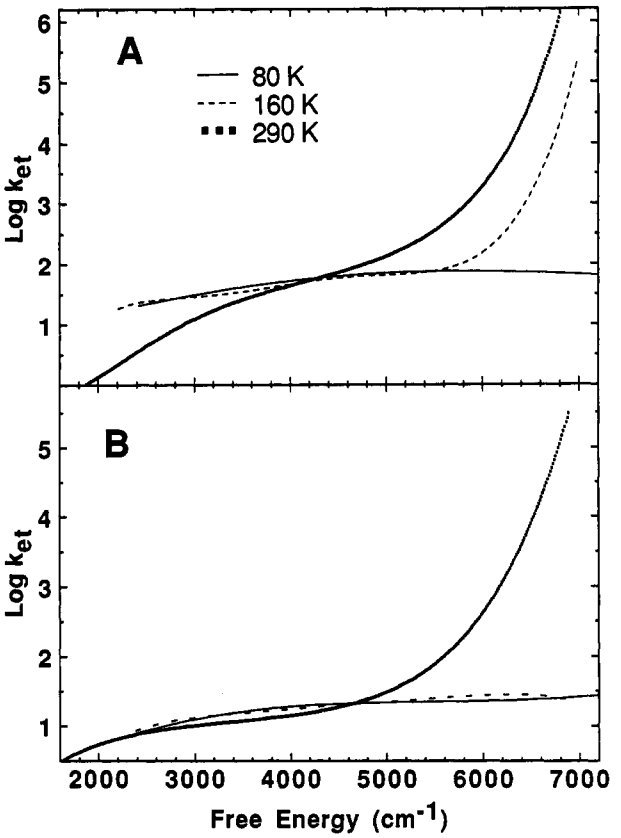

Figure 8. Comparison of the rate vs free-energy curves at 80 (—), 160 (- - -), and 290 K (– –). The curves have been corrected for the local field correction based on the relative value of the local field correction shown in Figure 6 and the temperature dependence of the free energy (see Table III). (**A**) The curves for population 1 show the increase in the activated process as the temperature is increased. (**B**) The curves for population 2 are very similar at 80 and 160 K. The curve at 290 K shows an activated region.

curves. For comparison with the curves obtained at 80 K, the interaction energy was corrected for the local field correction by multiplying by 1.06 at 160 K and 1.2 at 290 K to obtain the $\log(k_{et})$ vs ΔG_{et} curves shown in Figure 8.

The origin of the differences between low and high temperature can be due to activated recombination pathway(s) and the temperature dependence of the quantum-mechanical rate constant. The latter must be included because activated recombination can account only for the acceleration in rate. The deceleration and changes nearest zero field can be explained by considering the temperature dependence of the reorganization energy and/or free energy. In order to separate contributions from the intrinsic CR rate constant from the indirect activated pathway, we focus first on the region of the free-energy curve near the zero-field free energy because there is no evidence for an activated reaction via P^+H^- at zero electric field.[32] This region is well approximated by the slope of the rate vs interaction energy curve (P_1 and Q_1 in Tables I at 160 K and III at 290 K). We use the temperature dependence of the free-energy change of $P^+Q_A^-$ CR measured in solution using delayed fluorescence[47] while bearing in mind that the free energy and entropy in PVA may be different from those measured in solution. Most of the temperature dependence in our measurements and those in ref 47 is near room temperature.

5.2. Temperature Dependence of the Reorganization Energy. In order to estimate the temperature dependence of λ, we use the value of the entropy for the $P^+Q_A^-$ CR reaction[47] to obtain ΔG_{et} at each temperature (Table III) combined with the slopes P_1 and Q_1 (obtained from Table I in ref 1 at 80 K, Table I at 160 K, and Table II at 290 K). Application of eq 7 gives a ratio $\lambda/\Delta G_{et}$ which increases with temperature in accordance with the increase

TABLE III: Temperature Dependence of the Reorganization Energy Based on the Transfer Coefficient α Obtained from Electric Field Effect Data and Free Energy from Delayed Fluorescence[47]

	P_1[a]	α[b]	ΔG_{et},[c] eV	λ,[d] eV
		Fast Rate Population 1		
80 K	0.7	−0.011 ± 0.001	−0.60	0.61 ± 0.02
160 K	1.1	−0.035 ± 0.002	−0.57	0.61 ± 0.03
290 K	4.1	−0.23 ± 0.01	−0.52	0.97 ± 0.04
	Q_1[a]	α	ΔG_{et}	λ
		Slow Rate Population 2		
80 K	0.30	−0.005 ± 0.002	−0.60	0.60 ± 0.02
160 K	0.90	−0.028 ± 0.003	−0.57	0.60 ± 0.03
290 K	2.10	−0.12 ± 0.04	−0.52	0.69 ± 0.06

[a] The cumulants P_1 and Q_1 are calculated using logarithm to base 10 and must be multiplied by 2.303 to be equal to χ_{G1} in eq 5. The errors in these cumulants are reported in Table I in ref 1, and 80 K, and in Tables I and II at 160 and 290 K, respectively. [b] The transfer coefficient α was calculated from eq A.1 in the appendix of ref 1; see also text after eq 7. [c] The temperature dependence of the free energy was extrapolated from the delayed fluorescence experiment in ref 47. The error in ΔG_{et} is reported to be 0.02 eV in ref 47. It is assumed that the free-energy change is the same for both populations of RCs and that the free energy is the same in PVA as in aqueous solution. [d] The value of λ is calculated using the value of the first cumulant P_1 or Q_1 and the free energy in column 3 substituted into eq 7. Errors were propagated using the error in α and ΔG in eq 7.

TABLE IV: Experimental and Calculated Temperature Dependence of the $P^+Q_A^-$ Charge Recombination Rate Constant at Zero Field

		calcd χ_{T1} using parameters at 290 K[a]		
population	exptl slope[b] (×10⁴)	Marcus Theory[c] (×10⁴)	entropy included[d] (×10⁴)	temp-dependent λ[e] (×10)
1 (fast)	−3.4 ± 0.6	24.0 ± 3.0	8.4 ± 4.2	−46.0 ± 30.0
2 (slow)	−8.8 ± 1.7	−1.2 ± 1.3	−9.3 ± 3.0	−17 ± 2.5

[a] The parameters used are those given in Table III at 290 K for each population (1 and 2). [b] The slope of the experimental $\log(k_{et})$ vs temperature data obtained in PVA films (data not shown). Calculated values using eqs 8, 9, or 12 are divided by 2.303 to be compared with this value. [c] Using eq 8. Values are divided by 2.303 to convert to base 10. [d] Using eq 9 and values of ΔG_{et} and ΔS_{et} from ref 47. [e] The calculated value using eq 12 assumes that all of the reorganization energy is outer sphere. This equation includes the contribution of the entropy from eq 8. For population 1, $\delta\lambda/\delta T \simeq 1.7 \times 10^{-3}$, and for population 2, $\delta\lambda/\delta T \simeq 3.8 \times 10^{-4}$.

of the slope (P_1 or Q_1) with temperature. Given that the change in ΔG_{et} with temperature is relatively small, the result shown in Table III is that λ increases with temperature.

5.3. Consistency of the Rate vs ΔG_{et} Curves at 80, 160, and 290 K. To test whether the suggestion that the reorganization energy is temperature dependence is consistent with the observed temperature dependence, the slope of the experimental $\log(k_{et})$ vs T curve (section 4.2) in column 1 of Table IV is compared to three models: (1) λ and ΔG_{et} are independent of temperature, (2) ΔG_{et} only depends on temperature, and (3) both λ and ΔG_{et} depend on temperature. The slope in the second column in Table IV is calculated using Marcus theory (eq 8) using the parameters obtained from the room-temperature data with no temperature dependence to λ or ΔG_{et}. The value calculated using this model has the wrong sign and is much too large. The slope in the third column is calculated including the entropy change of the $P^+Q_A^- \rightarrow PQ_A$ reaction (eq 9). By including the entropy, better agreement with the temperature dependence is obtained (column 3). If the temperature-dependent reorganization energy is included as well as the entropy (column 4), the slope has the right sign for both populations, but the magnitude is not correct and the propagated error of the values in the column is relatively large. This model, which includes the temperature dependence of the reorganization energy at the level of Marcus theory (eq 6), does not fit the data quantitatively as a function of both free energy and temperature. There are several possible reasons for this. (1) The magnitude of $\partial\lambda/\partial T$ is not known accurately. The dependence of the reorganization energy on temperature can only be estimated from the calculations in Table III. (2) The free energy and entropy for the two populations may be different. (3) The amplitude of the populations also varies as a function of temperature. The slower process has a larger relative amplitude at higher temperature. For lack of a model to explain this, we have ignored the covariance between the relative amplitude and rate constant in the biexponential fit to the data. (4) The temperature dependence of the electronic factor has been neglected. (5) The temperature dependence of the local field has not been included. If the local field correction at 290 K is $f \simeq 1.2$, the value of the first cumulant is $P_1 = 3.40$ and $Q_1 = 1.75$, and the values of λ are 0.85 and 0.65 eV for populations 1 and 2, respectively. When corrected for the (upper bound) local field, the first cumulant in temperature is $\chi_{T1} \simeq -10^{-4}$ for population 1 and $\chi_{T1} \simeq -10^{-3}$ for population 2. In spite of these quantitative problems, a reorganization energy that increases with temperature is consistent with the steeper rate vs free-energy curve observed at higher temperature. Using Marcus theory, a larger reorganization energy at higher temperature predicts a larger barrier to recombination and a slower rate, as observed. This explanation for the observed temperature dependence may also explain such observations as a difference in $P^+Q_A^-$ recombination when RCs are frozen in the dark vs in the presence of saturating light.[72] In the latter case, the solvent configuration(s) with a larger λ may be frozen as well, leading to the slower observed rate. A temperature-dependent reorganization energy can explain a variety of observations and is more plausible than a temperature dependence to the electronic factor.[12]

5.4. Application of Multiphonon Electron-Transfer Theory. Marcus theory has the advantage of clarity in the application to both electric field and temperature-dependent data. The expansion of Marcus theory in powers of ΔG_{et} is clearly of limited utility since at most only two terms are obtained. In multiphonon treatments, the modes are partitioned into molecular (inner sphere) modes λ_{inner} and solvent (outer sphere) modes λ_{outer} such that $\lambda = \lambda_{inner} + \lambda_{outer}$. For high-frequency modes, $\lambda_{inner} = \sum_n S_n\omega_n$ where S_n and ω_n are, respectively, the electron–phonon coupling constant and the frequency of mode n. Solvent modes are represented by a polarization coordinate (λ_{outer}). A fit of the data to a quantum-mechanical ET theory at each temperature can serve to estimate the relative fraction of high- and low-frequency modes (see ref 1) at each temperature and, thereby, to learn which fraction of the reorganization energy is temperature dependent.

Using the same model as was applied to the data at 80 K, the rate vs free-energy curves at 160 and 290 K can be fit to a multiphonon theory using the saddle-point approximation.[1,45] In order not to include the region with the steep increase in rate (due to activated recombination via another electronic state P^+H^-; see below), only the data in the interaction energy range from −2200 to 600 cm^{-1} were fit to the multiphonon theory. In the fit, both the frequencies and electron–nuclear couplings were allowed to vary. The electron–nuclear coupling constants, frequencies, and reorganization energy are given in Table V. The trend of increasing reorganization energy with increasing temperature is seen in Table V just as was seen in Table III using only the first cumulant to analyze the data. The reorganization energy calculated using the saddle-point approximation is larger at all temperatures than using Marcus theory. The low-frequency component (due to modes of less than 200 cm^{-1}) of the reorganization energy increases as a fraction of the total as the temperature increases. This is reasonable since it is the solvent modes which are thought to be most temperature dependent. For

TABLE V: Parameters from the Fit of the Rate vs Free-Energy Curves to a Multiphonon Theory of Electron Transfer

	Fast Rate Population 1				Slow Rate Population 2			
	80 K[b]	160 K	290 K[c]	σ/Y[d]	80 K[b]	160 K	290 K	σ/Y[d]
S_1	2.8	3.3	2.7	0.04	1.4	1.9	2.2	0.04
ω_1[a]	1360	1870	1510	0.04	2820	2640	2550	0.03
S_2	44.7	57.0	120.0	0.01	14.4	16.8	12.1	0.01
ω_2[a]	58.0	33.0	50.0	0.05	265.0	171.0	213.0	0.04
λ, cm^{-1}	6450	8780	10 090	0.08	7790	8000	8290	0.06
λ, eV	0.80	1.09	1.25	0.08	0.97	0.99	1.03	0.06

[a] Frequencies in cm^{-1}. [b] These values differ from those in ref 1 because the free energy assumed there was $\Delta G_{et} = 0.52$ eV.[47] [c] Due to the steepness of the curve, a fit which retained reasonable values of the frequency was not possible. The values shown here represent a reasonable model of the data using the frequencies obtained in ref 1 and varying only S_i. [d] The standard deviations were determined from the covariance matrix from a nonlinear least-squares fit using the Marquardt algorithm. The relative errors are quite similar at all temperatures and are reported as the fractional error (σ/Y where Y is S_n, ω_n, or λ).

example, if the solvent component is treated using dielectric continuum theory, the temperature dependence of low-frequency modes is expressed by eq 11, where the change as a function of the temperature is described by the temperature dependence of the dielectric constant.[49]

Both Marcus theory and a multiphonon theory are consistent with a barrier height ΔG^* which increases with temperature. The activation barrier at zero field changes from approximately 100 ± 20 and 300 ± 60 cm^{-1} at 80 K to 700 ± 200 and 500 ± 100 cm^{-1} at 290 K for populations 1 and 2, respectively. The interpretation of the temperature dependence as being due to the lack of an activation barrier[12] is perhaps correct at temperatures below 80 K, but the discrepancy between theory and experiment is likely due to the change in barrier height as well as other factors near room temperature.

6. Discussion

6.1. Comparison with Other Electric Field Effect Experiments. Electric field effects on the rate for CR of $P^+Q_A^-$ have been reported by two other groups, but only at room temperature. Popovic et al. reported the electric-field-dependent kinetics on $P^+Q_A^-$ recombination in Langmuir–Blodgett (LB) films.[33] Gopher et al.[26] and Feher et al.[32] reported the use of an electrochemical cell to generate electric fields across a membrane containing RCs. In the latter case, the signal was monitored by observing a current transient after the excitation flash. The results obtained by these two methods do not agree. The current transient was observed to be single exponential in agreement with the single-exponential kinetics of $P^+Q_A^-$ recombination in solution.[53] The kinetics in LB films at zero field were different from those reported in solution in ref 33 and were fit to three exponentials.[54] The kinetics of the sample in LB films do not correspond to components of $P^+Q_A^-$ decay reported elsewhere.[26,42,53] The magnitude of the electric field effect on the rate constant in ref 33 was much smaller for all three components than that observed by Gopher et al.[26,32]

The electric field effect data at 290 K reported here agree with those in ref 32 over the region of free energy where they overlap. The slope and curvature of the rate vs free energy for both populations 1 and 2 in PVA agree within the experimental error with the single rate vs free-energy curve of both ubiquinone and AQ reported in monolayers in a solution cell.[32] The data using AQ-substituted RCs in ref 32 demonstrate an activated process in the applied electric field similar to that observed in our samples. The slope of the linear free-energy dependence of AQ reported in ref 32 agrees within the signal-to-noise of the data with the corresponding segment of the rate vs free-energy curves at 1600 ± 400 cm^{-1} in Figure 7 at 290 K (for both populations 1 and 2).

The origin of the discrepancy with the data in ref 33 may be the calibration of the electric field, which was accomplished using the sample capacitance and an assumed dielectric constant $\epsilon \simeq 3$. If the dielectric constant were larger, the field would be correspondingly smaller. The absence of evidence for an activated pathway raises serious questions about the calibration of the field as has previously been suggested in ref 32. It has recently been reported that if lauryldimethylamine *N*-oxide is the detergent, as in ref 33, the RCs in the LB film are not oriented.[55]

6.2. Comparison with Quinone Substitution Experiments. Although the $P^+Q_A^-$ CR reaction in native *Rb. sphaeroides* does not have an activated temperature regime, experiments with quinone replacements have shown that a 150-meV increase in energy is enough to cause the $P^+Q_A^-$ CR reaction to become activated at room temperature due to the proximity in energy to the state P^+H^- (see Figure 1).[24] Both AQ-substituted *Rb. sphaeroides* RCs and *Rps. viridis* RCs with their native Q_A have similar energy gaps between the state $P^+Q_A^-$ and P^+H^- and similar temperature dependences to the CR rate with an activated region at high temperature and an activationless region at low temperature.[23,43]

A comparison of the electric field effect results with data for RCs substituted in the Q_A binding site with a wide range of quinones is plotted in Figure 9. The data shown in square boxes were taken from refs 8 and 25. The low-temperature CR kinetics of substituted quinones are independent of temperature between 5 and 113 K.[8] The room-temperature free energies of the quinones were measured using delayed fluorescence.[25,56] Gunner et al. assumed that the free energy does not change as a function of temperature, although this appears not to be true for ubiquinone or AQ.[25,47] As discussed in ref 57, the scatter in the quinone-substitution data is relatively large. The rate vs free-energy curve at 80 K is placed between the two families of quinones identified by Gunner et al.[8] Both families of quinones have a shape similar to the rate vs free-energy curve, as do the 80 K electric field effect data. The main point of Figure 9 is that the rate vs free-energy curve obtained from quinone substitution is steeper at 300 K than at 113 K, in agreement with the results obtained here for $P^+Q_A^-$ CR at 290 and 80 K using an electric field perturbation. A straight line fit of the quinone data in the region $\Delta U = \pm 1300$ cm^{-1} gives a slope of 4 ± 0.8 eV^{-1} at 290 K and 1.2 ± 0.3 eV^{-1} at 80 K. Comparing these values to P_1 and Q_1 (in Table II of this work and Table I in ref 1 at 290 and 80 K, respectively), the quinone substitution data support the conclusion reached here that the direct $P^+Q_A^-$ charge recombination reaction is more dependent on free energy at 290 K than at cryogenic temperature.

In the region $\Delta U > 1300$ cm^{-1}, the activated process (via P^+H^-) contributes to the rate constant. The difference dipole moment for this activated process is smaller than for direct $P^+Q_A^-$ CR.[58] Thus, a comparison of the electric field effect data with data for quinone-substituted RCs (Figure 9) should show a systematic difference. Note that the energy scale in Figure 9 was calculated using the difference dipole moment of the $P^+Q_A^-$ state. However, altering the chemical nature of the quinone acceptor may also affect the relaxation of the $P^+Q_A^-$ dipole and thus the energy gap between $P^+Q_A^-$ and P^+H^-. For a number of quinones, a correlation has been observed which suggests that the energy of the state P^+H^- is ca. 0.5 eV (4000 cm^{-1}) above the energy of the $P^+Q_A^-$ state at room temperature,[24] a value that may be explained by a highly relaxed form of P^+H^-.[24] Because the time scale of the

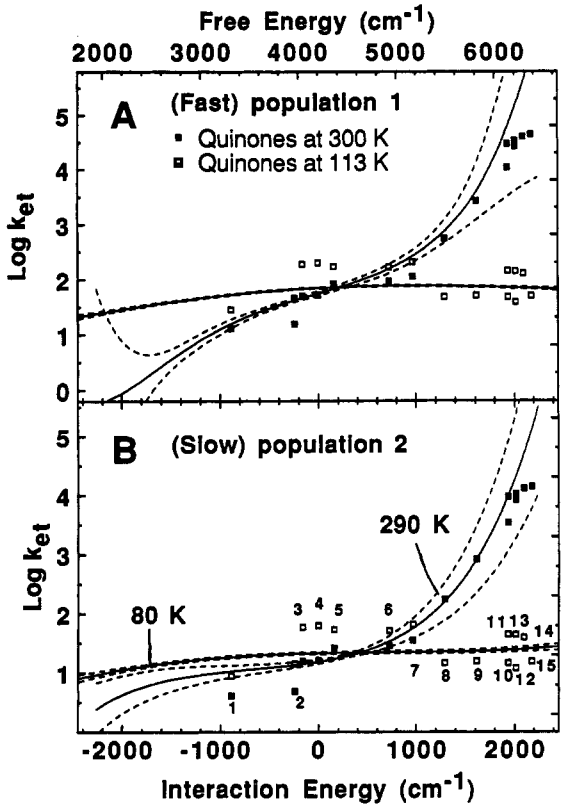

Figure 9. Comparison of the rate vs free-energy curves at 80 and 290 K with quinone substitution data at 113 and 300 K. (A) Electric field effect data for the faster population are compared to the rate constant measured for nonnative quinones substituted into the Q_A binding site. The rate constants of quinones at 113 K[8] are represented by hollow squares, and those at 300 K[25] for the same quinone are represented by vertically displaced filled black squares. The rate vs free-energy curves shown are derived from Figure 3 of ref 1 (80 K) and Figure 5 (290 K). (B) Electric field effect data for the slower population are compared to the rate constant of nonnative quinones.[8,25] The quinones are (1) *o*-naphthaquinone (o-NQ), (2) tetramethylbenzoquinone, (3) NQ, (4) UQ-10 (native), (5) menaquinone, (6) 2,3,5-trimethyl-NQ, (7) 5-methoxy-NQ, (8) AQ, (9) 1-methyl-AQ, (10) 1-methoxy-AQ, (11) 2-methyl-AQ, (12) 2-ethyl-AQ, (13) 2-dimethylamino-AQ, (14) 2-methoxy-AQ, and (15) 1-amino-AQ. The quinone data in the panels are identical and are plotted using a shifted ordinate to facilitate comparison.

activated recombination due to the effect of an applied electric field at room temperature is the same as that of the substituted quinones, we will also use the energy estimate of Woodbury et al.[25] for this relaxed form of the P^+H^- state in the following discussion. The next section addresses the question of the nature of the correlation between electric field effect and quinone substitution experiments in the region of activated recombination.

6.3. Activated Recombination Induced by an Electric Field. In order to estimate the contribution of the activated reaction via P^+H^- to the $P^+Q_A^-$ CR rate, the rate vs free-energy curves obtained in section 5.3 can be used to calculate parameters for the quantum-mechanical rate constant for the direct CR process $k_R(F)$. By contrast, the activated pathway, $k_{act}(F) = K_{-Q}(F)k_S(F)$, is described by an electric-field-dependent equilibrium constant $K_{-Q}(F)$ and rate constant $k_S(F)$, which are defined by eq B.4 in Appendix B for $P^+Q_A^-$ CR such that $k_{et}(F) = k_R(F) + k_{act}(F)$. The value of $k_R(F)$ is determined based on the fit to the interaction energy region between −2200 and 600 cm^{-1} in Figure 7. Activated recombination is calculated based on the portion of the curve with $\Delta U > 1300$ cm^{-1} using an extrapolated value of $k_R(F)$ and field dependence of $K_{-Q}(F)$ due to the difference dipole moment $\Delta\mu_Q = \mu(P^+Q_A^-) - \mu(P^+H^-)$, which is assumed to be the primary factor giving rise to the large acceleration in rate.

The activated recombination rate observed in an applied electric field is quantitatively larger than expected based on the known energetics of the states $P^+Q_A^-$ and P^+H^-. When the realistic values of $\Delta\mu_Q \simeq 50$ D, $\Delta G_Q \simeq 4000$ cm^{-1}, and field-independent $k_S(0) = 5 \times 10^7$ s^{-1} are included in a calculation of the rate vs free-energy curve including an activated pathway, there is no change predicted at 160 K and only a small activated rate obtained at 290 K even at the highest applied electric fields. The observed activated recombination is much larger at all temperatures above 160 K than that calculated using these parameters. If $f > 1$, better agreement is obtained because the equilibrium constant $K_{-Q}(F)$ is more strongly field dependent (see eq B.4). However, in order to get a calculated $k_{et}(F)$ which agrees with the experiment, the product $\Delta\mu_Q \cdot f$ in $K_{-Q}(F)$ must be 130 D, which is near the maximum possible value ($\Delta\mu_Q$ cannot be greater than the $P^+Q_A^-$ dipole, $\mu(P^+Q_A^-) \simeq 130$ D). Using this upper bound value of $\Delta\mu_Q$, agreement with the curves in Figure 7 is obtained if the free energies are $\Delta G_Q = 4200$ cm^{-1} for population 2 and $\Delta G_Q = 3800$ cm^{-1} for population 1. These values are consistent with the energetics of the P^+H^- state obtained from AQ-substituted RCs (see section 6.1). These free-energy differences between the two populations account for the difference in the activated rate in populations 1 and 2 at 160 and 290 K and are in agreement with evidence that there is a difference in energy between the two populations which have different $P^+Q_A^-$ CR rate constants.[59]

The observation that an upper bound value of $\Delta\mu_Q \simeq 130$ D (with $f = 1$) had to be used in the above calculation suggests that we cannot ignore the field dependence of $k_S(F)$ due to the difference dipole moment $\Delta\mu_S \simeq \mu(P^+H^-) - \mu(PH)$. If the field dependence of the state $k_S(F)$ is included up to the first (linear) cumulant to give $k_S(F) = \exp\{R_0 + R_1\Delta\mu_S \cdot F\}$ (using the notation R_n for the nth cumulant of this process), the activated recombination rate can be written as

$$k_{act}(F) = \exp\{R_0 - \Delta G_Q/kT + (R_1\Delta\mu_S + \Delta\mu_Q \cdot f/kT) \cdot F\} \quad (13)$$

If $R_1 > \Delta\mu_Q/[\Delta\mu_S kT]$, this model can account for the electric-field-induced activated recombination. Independent experimental evidence of the field dependence of $k_S(F)$ must be obtained to determine if this condition is met.

6.4. Origin of the Temperature-Dependent Reorganization Energy. The solvent reorganization energy in ET proteins may depend on the coupled motion of protons on titratable or hydrogen-bonded residues of the protein. The role of titratable residues near the Q_A and Q_B binding sites has been investigated by isotopic substitution and kinetics,[23,60] ENDOR,[61] and proton uptake.[62] Proton uptake studies show that approximately 1.0 proton is taken up when $P^+Q_B^-$ is formed and 0.4 proton is taken up on average when $P^+Q_A^-$ is formed.[62] One hypothesis is that proton uptake events may be responsible for the relaxation of the $P^+Q_A^-$ state energy. If the extent of proton uptake is temperature dependent, there may be a connection between proton uptake and the temperature-dependent reorganization energy of the CR reaction. However, recent electrogenicity measurements indicate that the direction of the charge displacement on the microsecond time scale is opposite to that required for proton uptake.[63] Furthermore, the free energy of the $P^+Q_A^-$ state shows only a mild dependence on the pH of the RC at room temperature (a change of about 0.03 eV is observed between pH 7 and 10[64-66]). The evidence suggests that there is a conformational change on the microsecond time scale which may solvate $P^+Q_A^-$ once it is formed,[66] but the details have not been elucidated.

Regardless of the detailed mechanism, the results presented here suggest that the $P^+Q_A^-$ state relaxes in energy on a time scale which is rapid compared to the recombination time k_R but slow compared to the k_S rate. Such a relaxation is consistent with a smaller energy gap between the $P^+Q_A^-$ and P^+H^- state (ΔG_Q) on the time scale relevant for activated recombination. This could explain why the electric field and quinone substitution

data are consistent with an energy gap which is 1000 cm^{-1} smaller than that estimated by delayed fluorescence measurements of ΔG_Q on the millisecond time scale.[47] If the solvation is temperature dependent, the relaxation of $P^+Q_A^-$ in energy is consistent with the temperature dependences of the free energy and reorganization energy which are found from the analysis of the electric field effect. The greater extent of solvation of the state $P^+Q_A^-$ by either reorientation of protein dipoles or proton shifts at higher temperatures leads to a smaller value of ΔG_{et} and a larger value of λ for the CR reaction at higher temperatures.

7. Conclusions

The strong dependence of the rate on electric field at 290 K is due to the presence of an activated recombination pathway, combined with a temperature dependence of the free energy and reorganization energy of the $P^+Q_A^-$ state. The magnitude that the rate constant for the $P^+Q_A^-$ charge recombination at zero field decreases at higher temperature can reasonably be explained by the assumption that the barrier to recombination is larger at higher temperature than at lower temperature. An analysis of the temperature dependence of the electric field effect has been modeled in terms of a temperature dependence of the reorganization energy. While quantitative issues remain (especially for the faster process), the hypothesis of a temperature-dependent reorganization energy can be used to explain several experimental results including the data in this paper and the observed difference in the $P^+Q_A^-$ charge recombination rate when RCs are frozen in the presence of saturating light.[24] The assumption that $P^+Q_A^-$ CR is activationless, based on the best fit to the temperature dependence of the $P^+Q_A^-$ CR reaction, is consistent with the electric field effect data at 80 K, but not at higher temperatures. The simplifying assumption that $\lambda \simeq -\Delta G_{et}$ at all temperatures[12] is likely not valid. Evidence was presented suggesting that the difference between the electric field effect at 80 K and room temperature may be in part due to relaxation events or conformational charges which solvate the $P^+Q_A^-$ dipole. This difference cannot be detected from the temperature dependence alone. This demonstrates that electric field effect experiments on the kinetics of electron-transfer reactions can be useful for determining whether measurements of the temperature dependence of ET accurately estimate the reorganization energy.

The results discussed here have implications for photosynthetic function. The role of the protein in the stabilization of charge is likely to be important, and it is likely that proton transfers are coupled to ET in photosynthetic RCs. The solvation of $P^+Q_A^-$ by the protein is probably related to the function of this state *in vivo* since the Q_A^- to Q_B reaction is controlled by the protonation state of the protein.[23] Given the sensitivity of the $P^+Q_A^-$ charge recombination rate to an applied electric field, it is also likely to be sensitive to the transmembrane potential. Therefore, the efficiency of ET from Q_A^- to Q_B depends on the interplay between the protonation state of the cytoplasmic side of the RC, which controls the forward charge shift rate,[23] and the transmembrane ΔpH driven by the light reactions of photosynthesis, which modulates the $P^+Q_A^-$ CR reaction.[67]

Acknowledgment. This work was supported in part by a grant from the NSF Biophysics Program.

Appendix A. Experimental Observation of Electric Field Effect on Steady-State Concentration

A.1. Probe Intensity Dependence of the Electric Field Effect. The origin of the baseline offset at long times in Figures 2–5 was investigated in the presence of the probe beam alone as a function of probe intensity, wavelength, and temperature. These probe-only experiments turn out to contain a considerable amount of additional information. They also are an example of a general class of experiments in which populations in an ET system are systematically manipulated and/or switched by an applied field. This class of experiments may prove to be of more widespread fundamental or applied interest.

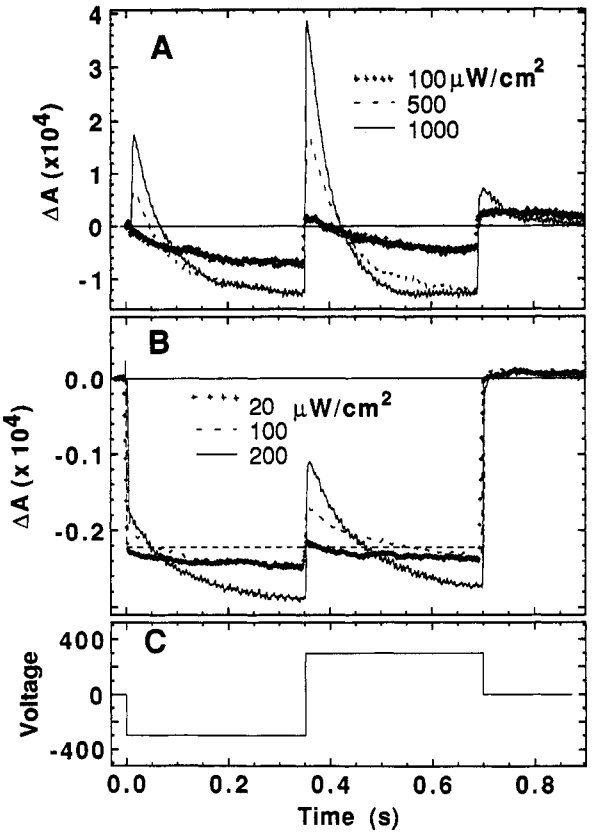

Figure 10. Electric field effects on $P^+Q_A^-$ population as a function of probe intensity and spectral bandwidth (F = 0.72 MV/cm, 290 K). (A) Dependence on probe intensity with a broad-band probe (~80 nm; without laser flash excitation). (B) Dependence on probe intensity with a narrow-band probe (5 nm centered at 870 nm; without laser flash excitation). The straight dashed line (- - -) represents the measured ac electrochromism at this wavelength. (C) Profile of the applied voltage.

In an applied electric field greater than 0.5 MV/cm and at temperatures above 140 K, large changes in the signal were observed for different broad-band probe intensities in the range 10 $\mu W/cm^2$ to 1 mW/cm^2 in the absence of flash excitation as shown in Figure 10. The sign and time course of ΔA shown in panels A and B are the same if the polarity of the voltage profile shown in panel C is reversed. With a probe intensity of $I = 100$ $\mu W/cm^2$, the change consists of a decrease in the absorbance following application of the field; however, for $I > 200$ $\mu W/cm^2$, there is an immediate increase in the absorbance of the P band which slowly changes to an absorbance decrease at longer times ($t > 100$ ms). The overall time courses for data with (Figure 3) and without (Figure 10) laser flash excitation are similar though not identical. A further feature in Figure 10A is the large change in absorbance which accompanies the change in the polarity of the applied electric field. This absorbance change is larger than that observed when the voltage is applied initially. In addition, there is a small change in the absorbance which accompanies the nulling of the voltage.

As shown in Figure 10B, if a narrow bandwidth probe source is used, the effects discussed in the previous paragraph are superimposed on an instantaneous offset which has a magnitude of $\Delta A = 2.2 \times 10^{-4}$; this electrochromism (electric-field-induced ΔA) is very large for the lowest electronic transition of P.[37,38] The intensity dependence for broad-band probe light in panel A is very similar to that obtained for the narrow band probe shown in panel B (lower probe intensities were used for the narrow band probe in order to keep the effect on the same scale as the electrochromism). Electrochromism (indicated by the straight

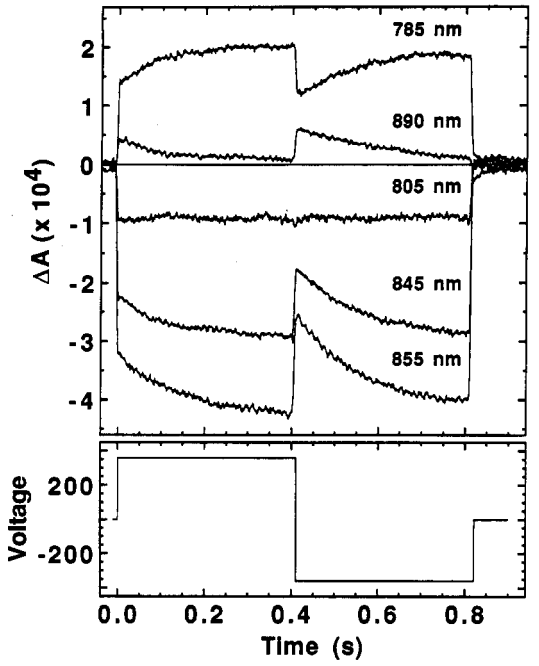

Figure 11. Dependence of the change in $[P^+Q_A^-]$ probed as a function of wavelength in an applied electric field. F = 0.64 MV/cm, and there is no laser flash excitation. Electric-field-induced ΔA at 290 K is shown as a function of time for selected wavelengths to demonstrate that the instantaneous offset (electrochromism) and kinetic changes do not have the same spectrum.

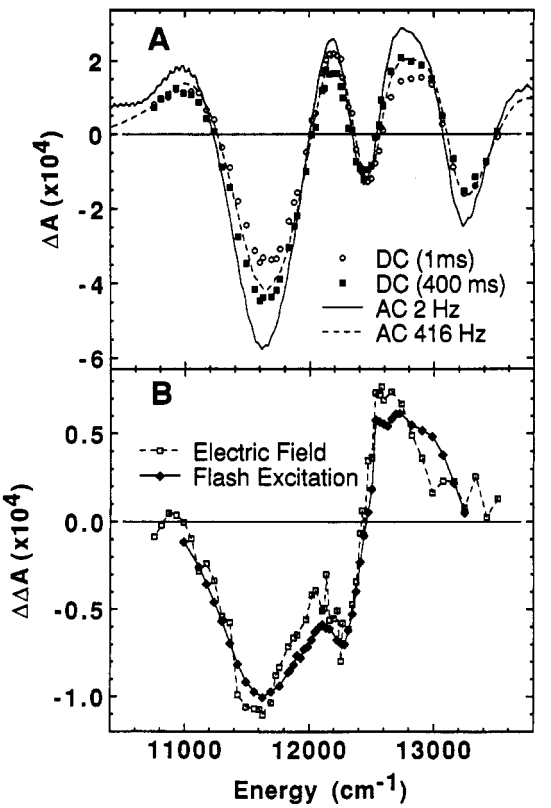

Figure 12. Comparison of the ac electrochromism and dc electric field effect experiments at 290 K (F = 6.4 × 10⁵ V/cm). (A) ΔA in a dc applied electric field measured at 1- and 400-ms delay times after the electric field application along with the ac. ΔA (electrochromism) using an applied electric field at 2 (—) and 416 Hz (- - -). (B) $\Delta\Delta A$ difference between the electric-field-induced change at 1 ms subtracted from that at 400 ms compared to a flash-induced difference spectrum. The latter is scaled in amplitude to the electric-field-induced spectrum for ease of comparison.

dashed line in Figure 10B) is not probe intensity dependent as long as the probe beam is not actinic (i.e., only a very small portion of the sample is in the $P^+Q_A^-$ state in the presence of the probe).

The probe intensity dependence shown in Figure 10 is not due to the intensity dependence of the electrochromism. As the probe beam intensity increases and appreciable saturation of the ground-state absorption of P occurs due to population of $P^+Q_A^-$, electrochromism in the P absorption band will decrease monotonically and linearly in proportion to the probe intensity until saturation is reached (assuming no new absorption grows in at the probe wavelength and the optical density of P is small, which is the present case). The time dependence of the electrochromism is exactly that of the applied dc field pulse and is proportional to the square of the applied field. The electric field effects as a function of intensity shown in Figure 10A and B are a highly nonlinear response to a square voltage pulse (Figure 10C). After a field application of 100 ms or more, ΔA increases with increasing probe intensity. The long time ($t > 0.5$ s) steady state is an absorbance change opposite in sign to that expected for saturation of the electrochromic effect. From Figure 10B, it is evident that the magnitude of the electrochromism is best measured at the lowest probe intensity possible. Low probe intensities ($I < 1$ $\mu W/cm^2$) are used routinely in ac measurements of electrochromism using lock-in detection.[37,38]

A.2. Time-Dependent Spectral Changes in an Electric Field. The identity of the state which gives rise to the electric-field-induced kinetic changes can be established by obtaining a time-dependent spectrum using a narrow band probe beam (shown in Figure 11 using a probe intensity of 100 $\mu W/cm^2$). The entire spectrum 1 and 400 ms after the field application is plotted in Figure 12A. The dc offsets at both 1 and 400 ms qualitatively resemble the ac electrochromism of P[37,38] also shown in Figure 12A. The kinetic changes in the dc signal suggest that ac electrochromism should show a frequency dependence at room temperature as shown in Figure 12A. To obtain the difference spectrum $\Delta\Delta A$ for the state giving rise to the kinetic changes, the electric-field-induced ΔA after 1 ms is subtracted from the ΔA after 400 ms, as shown in Figure 12B. $\Delta\Delta A$ obtained in an applied electric field has the appearance of the flash-induced $P^+Q_A^-$ difference spectrum. The comparison of these spectra suggests strongly that it is the population of the $P^+Q_A^-$ state in the presence of a probe beam which is affected by the application of an electric field.

A.3. Electric Field and Temperature Dependence of the $P^+Q_A^-$ Steady-State Concentration. The intensity dependence of the electric field effect proves that this is a change in the steady-state concentration of $P^+Q_A^-$ (cf. eq B.5 in Appendix B) rather than population of the state $P^+Q_A^-$ by an electric-field-induced shift in the equilibrium constant of the reaction $P^+Q_A^- \rightarrow PQ_A$ (cf. eq B.9). The absence of any population of the state $P^+Q_A^-$ due to an electric-field-induced shift in the equilibrium constant for the $P^+Q_A^- \rightarrow PQ_A$ reaction has also been shown using an electric field pulse/actinic probe experiment. In this experiment, the sample is kept in the dark while an electric field is applied. After a time (ranging between 0.4 and 1 s), the field is turned off and a shutter is opened, allowing a subsaturating actinic probe beam to interrogate the sample for 3 ms. The amplitude of the actinic probe at zero field and high field is compared to discern whether there is any change. This experiment was performed at several wavelengths characteristic of the $P^+Q_A^-$ difference spectrum. The result was negative, indicating that at fields as high as 8 × 10⁵ V/cm at 290 K there was no evidence for population of the state $P^+Q_A^-$ due to an applied electric field in the dark. Since the observed changes in rate and steady-state population are largest at 290 K, it was concluded that an electric-field-induced change in the equilibrium constant $K_{-R}(F)$ is negligible.

The response to an applied electric field as a function of temperature using a narrow bandwidth probe at 870 nm is shown in Figure 13 at two different probe intensities. The data plotted

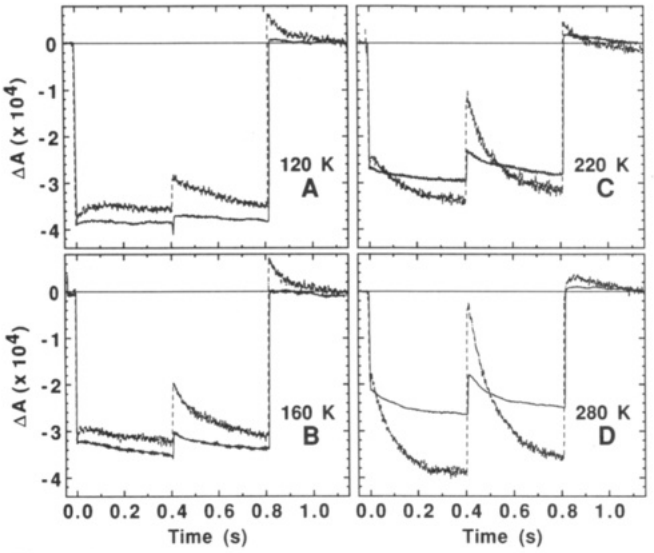

Figure 13. Temperature dependence of the effect of an electric field at high, I = 400 μW/cm^2 (- - -), and low, I = 40 μW/cm^2 (—), probe intensity (5 nm bandwidth centered at 870 nm; F = 0.64 MV/cm). (**A**) 120 K, (**B**) 160 K, (**C**) 220 K, (**D**) 280 K.

using a dashed and solid line in Figure 13 were obtained with probe intensities of 40 and 200 μW/cm^2, respectively. The instantaneous change in absorbance due to an applied electric field with no laser flash excitation (dashed line in Figure 10B) was also observed to have a temperature dependence similar to that of ac electrochromism.[38] The kinetics of the time-dependent absorbance changes in the first few hundred milliseconds after an electric field is applied show a much stronger temperature dependence. In Figure 13A, the data at 120 K have small changes relative to the higher temperatures. The instantaneous positive ΔA and the trend toward a negative ΔA at longer times grow larger as the temperature is increased to 160, 220, and 280 K in Figure 13B, C, and D, respectively. The fact that a negative ΔA is the sign of the steady-state change in an applied electric field indicates that the average rate constant for electron transfer from $P^+Q_A^-$ to the ground state slows down as the temperature is increased. This is true despite the large increase in rate constant observed in some orientational subpopulations (see Figures 4 and 5).

The trends in the data as a function of temperature can be summarized as follows. At low temperatures, there is essentially no absorbance decrease (further bleaching of P) on the hundreds of milliseconds time scale such as that observed at 220 and 280 K. The increase in absorbance at short times is seen most clearly at low temperatures but is present at all temperatures. This increase in ground-state absorption may be due either to quantum yield failure of one of the two reactions required to reach the state $P^+Q_A^-$ [68] or some orientations of the $P^+Q_A^-$ dipole which have a more rapid recombination rate constant (activated recombination discussed in section 6.3). In order to establish quantum yield failure, electric field effect experiments have been done in which the voltage was applied prior to a laser flash. These experiments are described elsewhere.[68]

A.4. Discussion. The time course of the response to the applied electric in Figure 10 needs more explanation. The increase in ΔA (the sharp spike evident after field application) is larger when the polarity of the applied voltage is reversed, than upon the initial application. This can be explained most simply by considering the two extreme orientations of the $P^+Q_A^-$ difference dipole $\Delta\mu_{et}$: those aligned with the electric field and those opposing the electric field direction. This is illustrated in Figure 14 where the extreme orientations (those most affected) are shown as the top and bottom sections of a circle which represents the sphere of dipolar orientations in an isotropic sample. The zero-field steady-state concentration is represented by the gray shaded area.

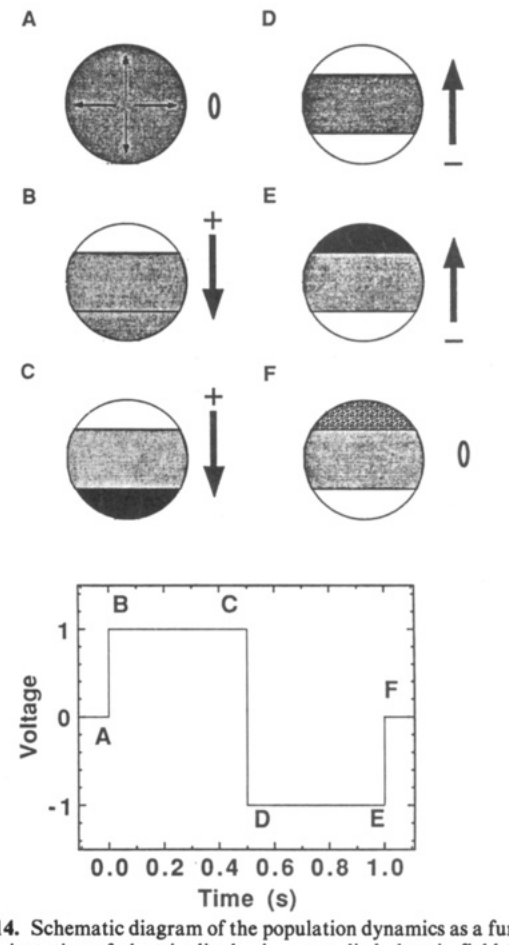

Figure 14. Schematic diagram of the population dynamics as a function of the orientation of electric dipoles in an applied electric field for an isotropic sample. The gray area represents the concentration of $P^+Q_A^-$ at zero field. The black and white areas represent orientations which have very high and very low steady-state concentrations, respectively. The time course of the field application is shown in the lower panel. (**A**) An isotropic distribution at zero field. (**B**) With **F** positive, opposing dipolar orientations (top) are depleted rapidly, while aligned orientations (bottom) approach the new steady-state value with a slow rate. (**C**) Aligned orientations have reached the steady-state value. (**D**) A rapid reversal of the polarity of **F** causes the new opposing dipolar orientations (bottom) to be rapidly depleted. The aligned orientations in negative **F** (top) had been depleted by the positive **F** and have not had time to achieve the new steady state. (**E**) The aligned orientations have reached the new steady state in negative **F**. (**F**) The anisotropic distribution of dipoles created by negative **F** decays with the zero-field rate constant.

The white area signifies a very low steady-state concentration (empty $P^+Q_A^-$ levels), and the black area signifies a high steady-state concentration (filled $P^+Q_A^-$ levels). At zero field, the sample is isotropic, shown by the gray circle in Figure 14A. Figure 14B shows the result of a field application. Those orientations of $\Delta\mu_{et}$ which oppose the field direction (increased in energy) result in the increase of ΔA immediately after the electric field is gated on (cf. the 1 mW/cm^2 data in Figure 10A) because the recombination rate constant is enhanced due to activated recombination and the steady-state concentration $\sigma I/[k_R(\mathbf{F}) + \sigma I]$ has become negligible. The dipoles aligned with the field have slow recombination rates, but the approach to steady state is also slow; thus, immediately after field application, the concentration for these orientations is unchanged. After 0.5 s, the steady-state concentration has built up to the new value as shown in Figure 14C.

The sign of the electric field (and thus the sign of $\Delta\mu_{et}\cdot\mathbf{F}$) is reversed in very short time (Figure 14D). Immediately after field reversal (Figure 14D), the empty $P^+Q_A^-$ levels (those which were high in energy before field reversal) are low in energy and have very slow rates. This population (top) approaches the (high) steady-state concentration with a slow rate. The filled $P^+Q_A^-$

levels (those which were low in energy before field reversal) are high in energy and reach their new depopulated steady state rapidly due to a very fast CR constant. Thus, the levels in *both* orientations of $\Delta\mu_{et}$ are depopulated as shown in Figure 14D. This explains why the change in ΔA upon field reversal is exactly twice as big as when the field is gated on from zero (as shown in Figure 10). After 0.5 s, the same steady-state concentration is reached for negative voltage as was reached for the positive voltage (Figure 14E). When the voltage is set to zero, all dipolar orientations have the same energy and decay with the same rate. There is small overshoot in the applied voltage which probably depletes some of the population in black area of Figure 14F. Thus, there is an increase in ΔA after the field is gated off (Figure 10). After several 1/e times at zero electric field, the sample is once again isotropic (Figure 14A). We note that this type of field reversal experiment is in itself a new approach to studying and manipulating ET reactions and may also offer the prospect of interesting technological applications.[69,70]

Appendix B. Calculation of the Electric Field Effect on the Steady-State Concentration

B.1. Electric Field Effect on the Kinetics. The probe beam introduces a pumping rate constant σI into the kinetic scheme of the RC, where σ is the absorption cross section and I the probe light intensity (see Figure 1). If σI is large relative to the charge recombination rate for a given state (e.g., k_R or k_S in Figure 1), that state is driven into saturation. In transient kinetics experiments, the probe beam is usually kept as weak as possible in order to avoid distorting the kinetic signal. If the system is disturbed from equilibrium by a saturating laser flash, the rate constant for approach to steady state is the sum of the forward and reverse rates $\sigma I + k_R$. In an electric field effect experiment, the rate constant k_R can slow significantly, thus changing the ratio $\sigma I/[k_R + \sigma I]$ which determines the steady-state concentration, and it can also distort the experimental observation of the rate constant k_R if the magnitude of k_R approaches σI.

The coupled differential equations which describe the change in population of the states shown in Figure 1 are given below.

$$\begin{aligned}
d[PHQ_A]/dt &= k_R(F)[P^+HQ_A^-] + \\
&\quad k_S(F)[P^+H^-Q_A] - (\sigma(F)I + k_{-R}(F))[PHQ_A] \\
d[P^+HQ_A^-]/dt &= -\{k_R(F) + \\
&\quad k_{-Q}(F)\}[P^+HQ_A^-] + k_Q(F)[P^+H^-Q_A] + k_{-R}(F)[PHQ_A] \\
d[P^+H^-Q_A]/dt &= -\{k_Q(F) + \\
&\quad k_S(F)\}[P^+H^-Q_A] + k_{-Q}(F)[P^+HQ_A^-] + k_1(F)[^1PHQ_A] \\
d[^1PHQ_A]/dt &= -k_1(F)[^1PHQ_A] + \sigma(F)I[PHQ_A] \qquad (B.1)
\end{aligned}$$

where, in principle, all of the rate constants are electric field dependent. The cross section $\sigma(F)$ of the P absorption band times the probe intensity I is a field-dependent pumping rate. Equilibria implicit in this scheme (e.g., $K_{-Q}(F) = k_{-Q}(F)/k_Q(F)$) are also electric field dependent.

The role played by spin states is not considered. In a general treatment of eqs B.1, the equation for the rate of change of the radical pair state P^+H^- must be solved using the stochastic Liouville equation.[71] Even if spin states were included, it is possible to state that the upper limit to charge recombination rate from the P^+H^- state is $k_S(F)$ (the rate constant for the singlet pathway of charge recombination from the radical pair state). Since both the rate constant k_S and the rate constant for intersystem crossing k_{isc} are orders of magnitude faster than $P^+Q_A^-$ charge recombination at zero electric field, to a first approximation we can assume that activated recombination leads to a much faster charge recombination regardless of spin.

B.2. Electric Field Effect on the Charge Recombination Kinetics of $P^+Q_A^-$. After laser excitation of the RC, the state $P^+Q_A^-$ is prepared with quantum yield of unity (in the absence of an electric field). Using this initial condition and the steady-state approximation for the states $[P^+H^-Q_A]$ and $[^1PHQ_A]$,

$$\frac{\partial[P^+H^-Q_A]}{\partial t} = 0 \quad \text{and} \quad \frac{\partial[^1PHQ_A]}{\partial t} = 0$$

the rate of return to the zero-field steady state with the field on is

$$k_{et}(F) = k_R(F) + k_{-Q}(F)(1 - \Phi(F)) + \sigma(F)I\varphi(F) \qquad (B.2)$$

where

$$\Phi(F) = \frac{k_Q(F)}{k_S(F) + k_Q(F)} \qquad (B.3)$$

This solution is valid for analysis of electric-field-modulated kinetics when the electric field is gated on immediately after the laser flash, i.e., after the steps which produce the species whose decay is monitored ($^1P \rightarrow P^+H^- \rightarrow P^+HQ_A^-$ in this case).

In order to clarify the role of the electric-field-dependent quantities, eq B.2 can be rewritten

$$k_{et}(F) = k_R(F) + K_{-Q}(F)k_S(F)\Phi(F) + \sigma(F)I\varphi(F) \qquad (B.4)$$

where $K_{-Q}(F) = \exp(-[\Delta G_Q - \Delta\mu_Q \cdot F]/kT)$, $\Delta G_Q = \Delta G(P^+H^-) - \Delta G(P^+Q_A^-)$ and $\Delta\mu_Q = \mu(P^+Q_A^-) - \mu(P^+H^-)$. The first term on the right-hand side of eq B.2 (or eq B.4) is the electric-field-dependent recombination rate constant for the two-level system in the absence of all other states. The second term is due to activated recombination, and the third term is intensity dependent.

In an external electric field, it is not possible to assume that the intensity-dependent erm in eq B.4 makes a negligible contribution. There is an intrinsic limit on the range of rates which can be sampled by the electric field effect on the reaction with a lower bound equal to $\sigma(F)I\varphi(F)$ in eq B.4. The contribution due to the intensity dependence of the rate constant is particularly important at room temperature where the slow process (recombination of population 2) has a rate constant of ca. 10 s^{-1}. If this rate constant slows by 1 order of magnitude to a rate constant of 1 s^{-1}, less than 10 $\mu W/cm^2$ probe intensity must be used in order not to drive a significant and orientation-dependent portion of the sample to steady state. It is possible to account for and exploit this experimental condition by including the steady-state concentration in the function used to fit the data.

B.3. Electric Field Effect on the $P^+Q_A^-$ Concentration. Using the steady-state approximation for the state $P^+Q_A^-$ at zero electric field, the difference between the concentrations of $P^+Q_A^-$ with and without an applied field F is

$$\frac{\Delta[P^+HQ_A^-]}{[PHQ_A]_{Tot}} = \frac{\sigma(F)I\varphi(F) + k_{-R}(F)}{[k_R(F) + k_{-Q}(1 - \Phi(F))] + \sigma(F)I\varphi(F)} - \frac{\sigma I}{k_R + \sigma I} \qquad (B.5)$$

where $[PHQ_A]_{Tot}$ is the total RC concentration and I is the light intensity.

B.4. Electric Field Effect on the Steady-State Concentration. The probe-intensity-dependent terms in eq B.5 describe electric-field-induced changes in the steady-state concentration of $P^+Q_A^-$ if the rate constant $k_R(F)$ and/or equilibrium $K_{-Q}(F)$ is highly field dependent. Assuming that $k_{-R}(F)$ is small (see Appendix A), the time-dependent change in the steady-state concentration in an electric field is obtained using the zero-field steady-state

concentration of $[P^+HQ_A^-]$ as the initial condition and orientation averaging:

$$\frac{\Delta[P^+HQ_A^-](t)}{[PHQ_A]_{Tot}} = \int_{-1}^{1}\left[\frac{\sigma(F)I\varphi(F)}{k_{et}(F)} - \frac{\sigma I}{k_R + \sigma I}\right]\times [1 - \exp\{-k_{et}(F)t\}]\, d(\cos\theta) \quad (B.6)$$

where $k_{et}(F)$ is given in eq B.4. The observed time course for approach to a new steady state is the same as for the decay of the bleach induced by a laser flash except that it is weighted by the field-dependent change in steady-state concentration (cf. Figures 5 and 10). For a system such as the RC where there are two populations, the amount of each population present at steady state will be weighted by the factors $\sigma I/[k_{R1} + \sigma I]$ and $\sigma I/k_{R2} + \sigma I]$. Using the experimental rate constants ($k_{R1} \simeq 15.1\ s^{-1}$ and $k_{R2} \simeq 53.7\ s^{-1}$) with their relative amplitudes, the slower population will contribute approximately 5 times more to the steady-state signal. We have shown elsewhere that it is justified to neglect the field dependence of $\Phi(F)$ in this expression.[68]

B.5. Electric Field Effect on the Equilibrium Constant. In the limit of zero probe light intensity, eq B.5 reduces to

$$\frac{\Delta[P^+HQ_A^-]}{[PHQ_A]_{Tot}} = \frac{k_{-R}(F)}{k_R(F)} \quad (B.7)$$

The electric-field-dependent equilibrium constant is $K_{-R}(F) = k_{-R}(F)/k_R(F)$. This equation gives the equilibrium thermal population of the state $P^+Q_A^-$ in an electric field in the dark. If the zero field free energy ΔG_{et} is known, then this equation provides a means to determine the local field correction. Using the principle of microscopic reversibility, we can write

$$\Delta[P^+HQ_A^-]/[PHQA]_{Tot} = \exp(-[\Delta G_R - \Delta\mu_R \cdot fF]/kT) \quad (B.8)$$

where f is the local field correction, $\Delta\mu_R \equiv \mu(P^+Q_A^-) - \mu(PQ_A)$, and effects due to the failure of quantum yield have been ignored. This equation can be orientation averaged analytically, yielding the electric-field-induced change in the equilibrium constant.

$$\frac{\Delta[P^+HQ_A^-]}{[PHQ_A]_{Tot}} = \exp\{-\Delta G_R/kT\}\times \left[\frac{\exp(\Delta\mu_R \cdot fF/kT) - \exp(-\Delta\mu_R \cdot fF/kT)}{\Delta\mu_R \cdot fF/kT}\right] \quad (B.9)$$

The time-dependent behavior of this signal is obtained by multiplying by $1 - \exp\{-(k_R(F) + k_{-R}(F))t\}$ and orientation averaging analogous to eq B.6. This result is important because it provides a means to determine the local field correction experimentally.[52]

References and Notes

(1) Franzen, S.; Goldstein, R. F.; Boxer, S. G. *J. Phys. Chem.* **1990**, *94*, 5135–5149.
(2) Marcus, R. A. *J. Chem. Phys.* **1965**, *43*, 679–701.
(3) Kitamura, N.; Okano, S.; Tazuke, S. *Chem. Phys. Lett.* **1982**, *90*, 13–17.
(4) Marcus, R. A.; Sutin, N. *Biochim. Biophys. Acta* **1985**, *811*, 265–322.
(5) Grampp, G.; Jaenicke, W. *Ber. Bunsenges. Phys. Chem.* **1984**, *88*, 335–340.
(6) Kuila, D.; Baxter, W. W.; Natan, M. J.; Hoffman, B. M. *J. Phys. Chem.* **1991**, *95*, 1–3.
(7) DeVault, D.; Chance, B. *Biophys. J.* **1966**, *6*, 825–847.
(8) Gunner, M. R.; Robertson, D. E.; Dutton, P. L. *J. Phys. Chem.* **1986**, *90*, 3783–3795.
(9) Using either semiclassical or multiphonon theories of ET because the condition of temperature independence holds for a wide range of values of λ as long as $\lambda > -\Delta G_{et}$. In addition, at low temperatures, the rate constant can be temperature independent due to the fact that modes coupled to ET are frozen out (nuclear tunneling in the normal regime).
(10) Liang, N.; Miller, J. R.; Closs, G. L. *J. Am. Chem. Soc.* **1989**, *111*, 8740–8741.
(11) DeVault, D. *Quantum-Mechanical Tunneling in Biological Systems*; Cambridge University Press: New York, 1984.
(12) Bixon, M.; Jortner, J. *J. Phys. Chem.* **1986**, *90*, 3795–3800.
(13) Holten, D.; Kirmaier, C.; Parson, W. W. *ACS Symp. Ser.* **1986**, *321* (Porphyrins: Excited States Dyn.), 205–218.
(14) Deisenhofer, J.; Epp, O.; Miki, K.; Huber, R.; Michel, H. *J. Mol. Biol.* **1984**, *180*, 385–398.
(15) Allen, J. P.; Feher, G.; Yeates, T. O.; Komiya, H.; Rees, D. C. *Proc. Natl. Acad. Sci. U.S.A.* **1987**, *84*, 6162–6166.
(16) Chang, C.-H.; Tiede, D.; Tang, J.; Smith, U.; Norris, J.; Schiffer, M. *FEBS Lett.* **1986**, *205*, 82–86.
(17) Goldstein, R. A.; Takiff, L. T.; Boxer, S. G. *Biochim. Biophys. Acta* **1988**, *934*, 253–263.
(18) Mar, T.; Vadeboncoeur, C.; Gingras, G. *Biochim. Biophys. Acta* **1983**, *724*, 317–322.
(19) Breton, J.; Martin, J.-L.; Fleming, G. R.; Lambry, J.-C. *Biochemistry* **1988**, *27*, 8276–8284.
(20) Kirmaier, C.; Holten, D.; Parson, W. W. *Biochim. Biophys. Acta* **1985**, *810*, 33–48.
(21) Kirmaier, C.; Holten, D. *Proc. Natl. Acad. Sci. U.S.A.* **1990**, *87*, 3552–3556.
(22) Fleming, G. R.; Martin, J.-L.; Breton, J. *Nature* **1988**, *333*, 190–192.
(23) Shopes, R. J.; Wraight, C. A. *Biochim. Biophys. Acta* **1987**, *893*, 409–425.
(24) Kleinfeld, D.; Okamura, M. Y.; Feher, G. *Biophys. J.* **1985**, *48*, 849–852.
(25) Woodbury, N. W.; Parson, W. W.; Gunner, M. R.; Prince, R. C.; Dutton, P. L. *Biochim. Biophys. Acta* **1986**, *851*, 6–22.
(26) Gopher, A.; Schonfeld, M.; Okamura, M. Y.; Feher, G. *Biophys. J.* **1985**, *48*, 311–320.
(27) Chidsey, C. E.; Kirmaier, C.; Holten, D.; Boxer, S. G. *Biochim. Biophys. Acta* **1984**, *766*, 424–437.
(28) Schenk, C. C.; Blankenship, R. E.; Parson, W. W. *Biochim. Biophys. Acta* **1982**, *680*, 44–59.
(29) Wraight, C. A.; Clayton, R. K. *Biochim. Biophys. Acta* **1973**, *333*, 246–260.
(30) Boxer, S. G.; Goldstein, R. A.; Franzen, S. In *Photoinduced Electron Transfer*; Fox, M. A., Chanon, M., Eds.; Elsevier Press: New York, 1988; Vol. B, pp 163–215.
(31) Boxer, S. G.; Lockhart, D. J.; Franzen, S. In *Photochemical Energy Conversion*; J. R. Norris, Jr., Meisel, D., Eds.; Elsevier Press: New York, 1989; pp 196–210.
(32) Feher, G.; Arno, T. R.; Okamura, M. Y. In *The Photosynthetic Bacterial Reaction Center: Structure and Dynamics*; Breton, J., Vermeglio, A., Eds.; Plenum Press: New York and London, 1988; pp 271–287.
(33) Popovic, Z. D.; Kovacs, G. J.; Vincett, P. S.; Alegria, G.; Dutton, P. L. *Biochim. Biophys. Acta* **1986**, *851*, 38–48.
(34) Gunner, M. R.; Tiede, D. M.; Prince, R. C.; Dutton, P. L. *Function of Quinones in Energy Conserving Systems*; Trumpower, T., Ed.; Academic Press: New York, 1982; pp 265–269.
(35) Feher, G.; Okamura, M. Y. In *The Photosynthetic Bacteria*; Clayton, R. K., Sistrom, W. R., Eds.; Plenum: New York, 1978; pp 349–386.
(36) Okamura, M. Y.; Isaacson, R. A.; Feher, G. *Proc. Natl. Acad. Sci. U.S.A.* **1975**, *72*, 3491–3495.
(37) Lockhart, D. J.; Boxer, S. G. *Biochemistry* **1987**, *26*, 644–668.
(38) Lösche, M.; Feher, G.; Okamura, M. Y. *Proc. Natl. Acad. Sci. U.S.A.* **1987**, *84*, 7537–7541.
(39) Böttcher, T. *Theory of Dielectric Polarization*; Elsevier: New York, 1973; Vol. 1.
(40) The $P^+Q_A^-$ CR process is observed to be biexponential,[1,41,42] and we have assumed that this corresponds to two populations which do not interconvert in the presence of an electric field. The CR rate constants at 290 K are $k_{R1} = 53.7 \pm 5.0\ s^{-1}$ and $k_{R2} = 15.1 \pm 1.2\ s^{-1}$ for populations 1 and 2, respectively. The relative amplitudes are 36% ± 9% and 64% ± 9% for populations 1 and 2, respectively.
(41) Parot, P.; Thiery, J.; Vermeglio, A. *Biochim. Biophys. Acta* **1987**, *893*, 534–543.
(42) Clayton, R. K.; Yau, H. F. *Biophys. J.* **1972**, *12*, 867–881.
(43) Sebban, P.; Wraight, C. A. *Biochim. Biophys. Acta* **1989**, *974*, 54–65.
(44) Sebban, P. *Biochim. Biophys. Acta* **1988**, *936*, 124–136.
(45) Franzen, S.; Lao, K.; Boxer, S. G. *Chem. Phys. Lett.* **1992**, *197*, 380–388.
(46) Marcus, R. A. *J. Chem. Phys.* **1984**, *81*, 4494–4500.
(47) Arata, H.; Parson, W. W. *Biochim. Biophys. Acta* **1981**, *638*, 201–209.
(48) Marcus, R. A.; Suton, N. *Inorg. Chem.* **1975**, *14*, 213–216.
(49) Debye, P. *Polar Molecules*; The Chemical Catalog Co.: New York, 1929.
(50) In order to apply eq 11 to the RC, we need to know what fraction of the reorganization energy is due to solvent polarization (outer sphere). λ_{outer} decreases as the temperature is lowered because there are fewer states accessible to protons or more hindered motion of dipoles.
(51) Pethig, R. *Dielectric and Electronic Properties of Biological Materials*; Wiley: Chichester, England, 1979.
(52) Experiments are described in Appendix A which probe the shift in equilibrium in an applied electric field and thereby allow an estimate of the local field correction. The electric field is gated on in the dark, and the electric-field-shifted equilibrium is detectable if the change in ΔA is at least 10^{-5}. Since the equilibrium constant for the reaction $PQ_A \rightarrow P^+Q_A^-$ is 10^{-9} at zero

field at 290 K, this requires a change in the equilibrium constant by a factor 10^4. At the highest field 8×10^5 V/cm, the interaction energy of 130-D dipole moment is approximately 1750 cm^{-1}. Using this value and eq B.9 from Appendix B, we conclude that $f < 1.3$ at room temperature.

(53) McElroy, J. D.; Mauzerall, D. C.; Feher, G. *Biochim. Biophys. Acta* **1974**, *333*, 261–277.

(54) Popovic, Z. D.; Kovacs, G. J.; Vincett, P. S.; Dutton, P. L. *Chem. Phys. Lett.* **1985**, *116*, 405–410.

(55) Alegria, G.; Dutton, P. L. *Biochim. Biophys. Acta* **1990**, *1057*, 258–272.

(56) All of the quinones from refs 8 and 25 were used except those which had no rate constant reported at 290 K and 1-chloro-AQ. The latter quinone has an *in vitro* redox potential of –0.15 and an *in situ* redox potential of 0.11 relative to native ubiquinone. Quantitative comparison is limited by the fact that many of the decays of quinone-substituted RCs are known to be biexponential but were treated as monoexponential in refs 8 and 25. In Figure 9, each population is compared separately to the average rate given in refs 8 and 25.

(57) Gunner, M. R.; Dutton, P. L. *J. Am. Chem. Soc.* **1989**, *111*, 3400–3412.

(58) Given the values $\mu(P^+H^-) \simeq 80$ D and $\mu(P^+Q_A^-) \simeq 130$ D, the difference dipole moment for activated recombination is at least 50 D [$\Delta\mu_Q = \mu(P^+Q_A^-) - \mu(P^+H^-)$]. For the angle of 22° between the two dipoles estimated from the three-dimensional structure,[14-16] the difference dipole is not much larger than 50 D.

(59) Baciou, L.; Rivas, E.; Sebban, P. *Biochemistry* **1990**, *29*, 2966–2976.

(60) Okamura, M. Y.; Feher, G. *Proc. Natl. Acad. Sci. U.S.A.* **1986**, *83*, 8152–8156.

(61) Lubitz, W.; Abresch, E. C.; Debus, R. J.; Isaacson, R. A.; Okamura, M. Y.; Feher, G. *Biochim. Biophys. Acta* **1985**, *808*, 464–469.

(62) McPherson, P. H.; Okamura, M. Y.; Feher, G. *Biochim. Biophys. Acta* **1988**, *934*, 348–368.

(63) Brzhezinski, P.; Paddock, M. L.; Messinger, A.; Okamura, M. Y.; Feher, G. *Biophys. J.* **1992**, *61*, a101.

(64) Equilibrium redox titrations show a larger dependence of ΔG_{et} on pH.[65]

(65) Maroti, P.; Wraight, C. A. *Biochim. Biophys. Acta* **1988**, *934*, 329–347.

(66) McPherson, P. H.; Nagarajan, V.; Parson, W. W.; Okamura, M. Y.; Feher, G. *Biochim. Biophys. Acta* **1990**, *1019*, 91–94.

(67) Wais, E.; Ball, J.; Berry, J. In *Progress in Photosynthesis Reasearch*; Biggens, J., Ed.; Martinus Nijhoff: Dordrecht, Netherlands, 1987; Vol. II, pp 553–556.

(68) Franzen, S.; Lao, K.-Q.; Lambright, D. G.; Boxer, S. G. *J. Phys. Chem.*, to be submitted.

(69) A somewhat related phenomenon was described many years ago by Bullot and Albrecht in glassy media.[70]

(70) Bullot, J.; Albrecht, A. C. *J. Chem. Phys.* **1969**, *40*, 289–300.

(71) Chidsey, C. E. D.; Takiff, L.; Goldstein, R. A.; Boxer, S. G. *Proc. Natl. Acad. Sci. U.S.A.* **1985**, *82*, 6850–6854.

(72) Kleinfeld, D.; Okamura, M. Y.; Feher, G. *Biochemistry* **1984**, *23*, 5780–5786.